Author's response on

"N₂O isotope approaches for source partitioning of N₂O production and estimation of N₂O reduction – validation with ₁₅N gas-flux method in laboratory and field studies" by Dominika Lewicka-Szczebak et al.

Review response for Anonymous referee #1

- $^{(1)}$ *comments from referees*
- $^{(2)}$ authors response
- $^{(3)}$ authors changes in manuscript

Thank you very much for your positive evaluation of the manuscript and your critical comments which helped us to improve our work.

We will take into account all the comments and especially clarify the endmembers isotope values corrections we applied. Here we provide detailed responses for the raised points, minor corrections have been accepted and will be included into reviewed manuscript.

L70 I am not sure if I understand correctly. The observed isotope effect for N2O reduction is quite stable and doesn't depend on r N2O. Do you mean "change in N2O isotopic composition due to N2O reduction depends largely on y n2o"?

Isotope fractionation during N2O reduction is independent of rN2O (mostly). But with the isotope effect we meant the change in N2O isotopic signature, as you suggest. To avoid confusion this will be changed in the manuscript to: 'the increase in $\delta^{18}O$, $\delta^{15}N$ and $\delta^{15}N^{SP}$ of the residual N_2O due to N_2O reduction, is related to r_{N2O}'

L77-78: I don't understand "N2O mixing ratio between two N2O production pathways and rN2O".

This will be changed to: 'N_2O mixing proportions of two N_2O production pathways and r_{N2O}'

Section 2.1: has this experiment been conducted in 2015/2016. Please confirm if this is the procedure that has been applied in the past and state clearly that this paper reports on past campaigns and current incubations of the same soil.

Yes, the field campaigns were conducted in 2015 and 2016, and the incubations in 2018. This information will be added: 'The soil for incubations, upper 30cm layer, was collected on the

Materials and Methods
L192 cf: On the one hand, water was added to obtain a certain water content in the soil. On the other hand, columns were continuously flushed with He/O2/N2. These gases are dry (i.e., very low dew points), so that they will take up significant amounts of water from the soil, considering a flush time of 5 days. As a consequence, the soil columns will dry out under this treatment. How did the authors account for this drying effect when referring to the WFPS values? Are the WFPS values an average or the initially values that was aimed at?

The WFPS was analysed with mineral nitrogen analyses and do not show significant decrease. The given WFPS values are the actual measured values, not the theoretical target values. The results are presented in the supplement (Fig.S1). Water was also added in the middle of the experiment therefore the drying effect was not significant. The reference to the WFPS results shown in supplement will be added in this section: 'The WFPS values were controlled during the experiment (Fig. S1).'

L210: I suggest mentioning that fluxes were calculated based on the dynamic chamber principle. Correction for the inlet concentration is omitted since the gas mixture used for flushing is N2O-free. Do I get this right?

Yes, thank you, this will be added.

L310: Please give a rationale for expecting higher fungal denitrification than Ni

This is rather high soil moisture (>60% WFPS) and low ammonium content (Table 1). This explanation will be added in the text.

L319: I suggest explaining what the cases are: Case 1 assumes reduction of N2O produced through bacterial denitrification and subsequent mixing, whereas case 2 assumes mixing and subsequent reduction of the mixed pool by denitrifiers. : : : if I am getting you right.

Yes, this is right, but this is just explained a few lines above. I would like to rather avoid repetitions.

L320: please explain c, and explain what happens if the condition is met.

Sorry, this was a mistake in properly displaying of this formula, it should be:
$L_{i+1}/L_i \geq \alpha$,
'c' was a typo.
The condition of $L_{i+1}/L_i \geq \alpha$ is the main concept of standard Metropolis algorithm. The newly generated state is accepted as a valid configuration if the likelihood function ratio L_{i+1}/L_i is greater or equal than a random variable α. If the state is accepted it becomes a new

reference (appearing in the denominator) in the next iteration. If it is not accepted the next iteration is performed with unchanged value in the denominator in likelihood ratios.

Results
L421-425: Actually, I can't follow this short statement entirely. I understand that the authors aim at getting rid of the implicit assumption of DELTAdelta maps that the dominant source of N2O is denitrification. I thank the authors for this advancement.

There was one mistake in this paragraph: wrong word 'precursor' was used instead of 'endmember' (L422), which probably made the understanding of this section difficult. We will correct this and further clarify the points below.

Some unclarities remain however:
1. For a 18O/SP map, the endmember values for bD, nD and fD are changed by the same amount, -6.4 per mil of water. Correcting for 18O of water makes sense, if nitrate exchanges O with water completely. However, when looking in the literature cited, it seems like the endmember values in the literature have been corrected for 18O already. For this reason, and I want to discuss this with the authors, I suggest correcting for the difference in d18O water between the presented study and the body of literature. Please clarify.

Since the O-exchange is usually high correcting with water makes more sense that with nitrate. Of course, if we knew the exact O-exchange this could be done more precisely, but usually it is not known. These effects and associated uncertainties are discussed in Section 4.1, L641-655. The cited literature values (Table S1) are the isotope effects – so, the isotope shift between the water applied and the emitted N2O – to avoid confusion we will denote this with ε:
$\varepsilon_{N2O/H2O} = \delta_{N2O} - \delta_{H2O}$, e.g. $\delta_{N2O} = 10$, $\delta_{H2O} = -9 \Rightarrow \varepsilon_{N2O/H2O} = 19$

We aim to calculate the expected N2O δ values emitted from the particular pathways for our case studies, with $\delta_{H2O} = -6.4$ so need to calculate:

$\delta_{N2O} = \varepsilon_{N2O/H2O} + \delta_{H2O} = 12.6$

All this values are presented in Table S1 in the supplement. But now I realise these are very important data for the study so this table will be moved to the main manuscript text and placed below the calculation explanations.

This more exact explanation will be added in the manuscript as well.

2. Again, for a 18O/SP map, this correction is equivalent with a correction of the measured N2O 18O signature with water 18O, as correcting all endmembers for the same value is mathematically the same as correcting the measured values.

We are not correcting all the endmembers with water, because $\delta 18O$ for Ni depends on atmospheric oxygen (since this is quite stable we do not assume stable value for this source). You are right – for the case of bD and fD mixing for SP/O Map it doesn't make difference but it does for bD-Ni mixing and for all results of the 3DI model.

3. For 15N/SP maps, this is actually a further development, since this allows correcting both Ni and bD, fD and nD endmembers, in contrast to only correcting measured values with one assumed precursor composition.
I am asking the authors to comment on this and make this clear in the text if they agree. Please also explain the sign of your correction. It interferes with the definition of the apparent isotope effect in your reference 4 of the supplementary material (Sutka 2006).

Thank you, this statement will be added in the manuscript. But this works for both SP/N and SP/O Map - because δ18O for Ni in this approach is not corrected with water but can be corrected to the atmospheric oxygen (if different than mean value, which may be the case in e.g. aquatic studies).

We will add the definition of ε to make the signs and recalculation procedures clear (the literature data is recalculated according to our definition). But I couldn't find the definition of the apparent isotope effect in (Sutka et al., 2006) and any supplementary material to this paper.

After addition of clarifications this paragraph will expand and will not fit anymore to results section. It will be moved to Methods section 2.5, as:

For the graphical presentation of dual isotope plots for sampling points always $\delta^{18}O$ and $\delta^{15}N$ values of emitted N_2O are plotted ($\delta^{18}O_{N2O}$, $\delta^{15}N_{N2O}$). But the precursors isotopic signatures ($\delta^{18}O_{H2O}$, $\delta^{15}N_{NO3-}$, $\delta^{15}N_{NH4+}$) are taken into account by respective correction of mixing endmembers isotopic ranges (see Table S1). The literature endmember ranges are given as isotope effects (ε) expressed in relation to particular precursor relevant for particular pathway, e.g. for $\delta^{18}O$ of bD the $\varepsilon_{N2O/H2O}$ is calculated by subtracting the precursor isotopic signature (δ_{H2O}) from the measured δ_{N2O} values:

$$\varepsilon_{N2O/precursor} = \delta_{N2O} - \delta_{precursor} \tag{11}$$

e.g. for $\delta^{18}O$ of bD: $\delta_{N2O} = 10$, $\delta_{H2O} = -9$; $\varepsilon_{N2O/H2O} = 19$

Afterwards, the literature isotope effects are corrected with the actually measured precursor values determined for the particular study ($\delta_{actual\ precursor}$) to determine the characteristic isotopic signature of N_2O emitted from the particular mixing endmember for this particular study conditions ($\delta_{N2O,\ endmember}$):

$$\delta_{N2O\_endmember} = \varepsilon_{N2O/precursor} + \delta_{actual\ precursor} \tag{12}$$

e.g. $\delta^{18}O$ of bD: $\varepsilon_{N2O/H2O} = 19$, $\delta_{actual\ H2O} = -6.4$, $\delta_{N2O\_bD} = 12.6$.

Hence, the endmember ranges represent the expected isotopic signatures of N_2O originating from each mixing endmember for the particular case study characterised by specific precursor isotopic signatures. Such approach allows for presenting all data in the common isotopic

scales without presumption on the dominating pathway and dominating precursor. Hence, this new approach presented here is actually a further development of Maps, since this allows for correcting both Ni and bD, fD and nD endmembers with relevant distinct precursors, in contrast to only correcting measured values with one common assumed precursor isotopic signature. In previous papers, where $\delta^{18}O$ and $\delta^{15}N$ related to precursors ($\delta^{18}O_{N2O/H2O}$, $\delta^{15}N_{N2O/NO3}$) were plotted (Ibraim et al., 2019; Lewicka-Szczebak et al., 2017; Lewicka-Szczebak et al., 2016) it was assumed that denitrification must be the dominating N_2O production pathway.

L434: Please define minimum reduction line. I guess it is the dashed red line, but it hasn't been defined in the figure caption.

This definition will be added, it is indeed the dashed line. Sorry for the missing information.

L461: there is a large discrepancy of field and laboratory NH4 delta values. This observation should also be taken up in the discussion again.

This is most probably due to differences in fertilizer addition techniques. In field studies the fertilizer solution was injected into the soil intact columns and in laboratory studies it was mixed and afterwards packed into the vessels. In both studies we observe a very fast decrease in ammonium content which is most probably due to its adsorption. The more detailed interpretation of 15N experimental results including Ntrace model is ongoing, but probably during mixing this adsorption process is more enhanced when compared to injection technique. But this is just a speculation so far. The discussion on this issue will be extended in the follow up paper, where we also include the 15N-NH4 treatment which was not presented here. This information will be added in the manuscript.

L495: In my opinion, the pie charts are i) not well described and ii) consume more space than necessary. If the authors stick to the pie charts, I ask them to indicate that the share of N2 produced during N2O reduction is given as N2 in percent. Hatched superimposed patterns show the source processes for N2O that has been reduced to N2. All in all, my suggestion is showing 2 bar plots (case 1 and case 2) with categories bD (bdN2O, bdN2), nD, fD, Ni, N2.

Thank you for the nice idea with bar plots. We hoped to nicely present the comparison between cases with the pie plots, but apparently did not succeed with this idea, we fully agree that bar plots are better for this aim. This will be changed and such new Figures will be included in the manuscript:
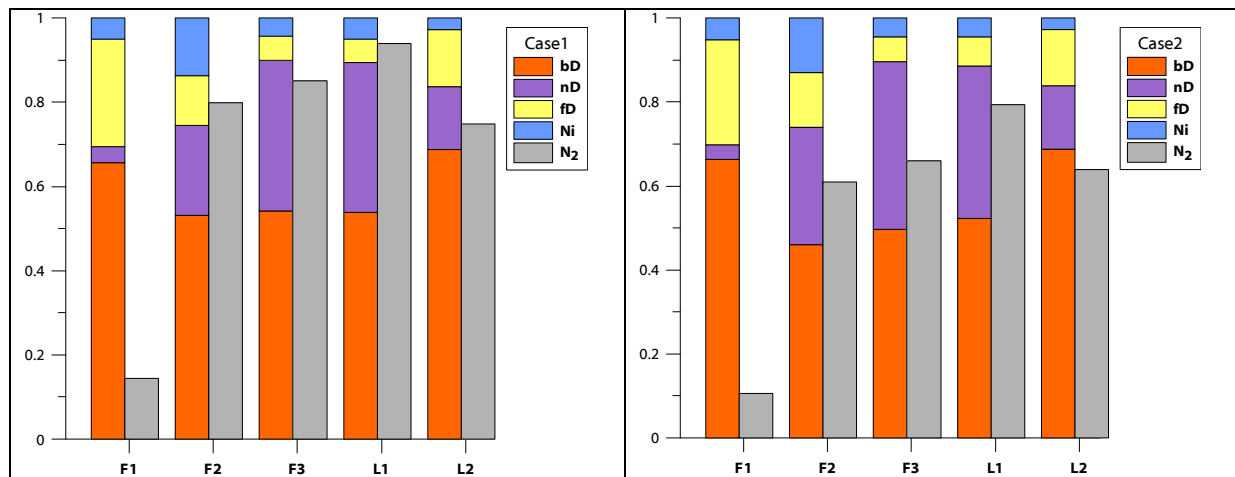
Figure 5: figure 5 gives everything but an overview of the results. I suggest showing only one case for Laboratory or field and instead have the numbers intelligible, and annotate scales. Please only show significant correlations, and don't correlate font size with correlation strength.

Ok, I see your points. I think we can fully move this Figure to the supplement. Since the number of points (individual iterations) is very high – ca. 1000 points – most correlations are significant, even showing low R values. These are also standard graphs for the isotope mixing models introduced by the trophic nets research and we wanted to keep the idea similar. Showing 2 graphs only will not be informative, and actually the needed information is referred in the text and all the graphs will be presented in the supplement.

L569: why is p<0.1 considered as significant? I suggest rephrasing the sentence, proved sounds odd in terms of statistical inference. The p agreement between reference method and SP/O Map (p<0.1??) as well as Case 2 of 3DI model (p<0.05) was statistically significant.

p<0.1 may be assumed as statistically significant, we have changed this in the statistical methods, Section 2.7. Although only p<0.05 is usually accepted as significant, here we think that the values obtained for SP/O Map are also important indication and should be accepted, with a clear statement that this statistical significance is weak (p values are shown). The sentence will be corrected.

Discussion L718-720: could the authors please explain how the uncertainty was actually transferred in the model. In line 331-332, the authors state that ": : :uncertainties of the source's data ifs fed into the model through the variance in the calculation of unnormalized likelihood". However, I don't understand then the following sentence, that the prior distribution was assumed uninformative. Does this mean that for each endmember isotopic composition, the whole range of values was allowed? Please clarify how this actually works.

The sentence 'the prior distribution was assumed uninformative' is misleading. It refers to starting values for the model – we do not assume any preference for any pathway, that's why flat Dirichlet distribution is applied. We will modify this sentence to avoid confusion.

We have applied the sources data with their uncertainty into the model, as defined in Tab S1.

Conclusion
L863-864: I think this needs to be rephrased. The authors haven't presented a triple isotope plot, but rather present a likelihood function that allows for including three isotopic quantities and 4 associated isotopic endmembers.

This sentence will be corrected to:

- Here we present for the first time the idea of applying a model based on three N_2O isotopic signatures. We are convinced that this is a powerful step forward in development of N_2O isotopocule methods to quantify especially r_{N2O}, but also estimate some mixing proportions of the four N_2O pathways included in the model.

Author's response on

"N₂O isotope approaches for source partitioning of N₂O production and estimation of N₂O reduction – validation with 15N gas-flux method in laboratory and field studies" by Dominika Lewicka-Szczebak et al.

Review response for Anonymous referee #2

- [(1)] *comments from referees*
- [(2)] authors response
- [(3)] authors changes in manuscript

Thank you very much for your positive evaluation of the manuscript and your critical comments which helped us to improve our work.

Line 61: It would be helpful to provide the actual value of sensitivity increase here so that a direct comparison can be made.

This is about 80-fold increase in sensitivity. This information will be added in the text.

Line 68: 'budget' is a more appropriate word here rather than emission. It is probably much easier to measure N2O fluxes directly if emission is intended.

Thank you, this will be changed.

Line 76: Should diffusion of N2O be taken into account as one of the processes determining the final N2O isotopes? Either here or in discussion, why the fractionation factor of diffusion is not considered in this study should be briefly mentioned.

We consider rather enzymatic processes than diffusion to be rate-limiting since enzymatic isotope fractionation is rather determining the apparent isotope effect. This has been more deeply discussed in our previous publications (Lewicka-Szczebak et al., 2014, 2015) and we will add this information here.

Line 98: What was the non-identical treatment here? Suggest briefly describe to give the readers some idea on the treatment differences which should be avoided

Different fertilizer application procedures: needle injection of fertilizer solution for ^{15}N treatments and surface distribution of fertilizer in NA treatments, different sizes of ^{15}N and NA microplots and chambers). This information will be added.

Line 117: Suggest the authors indicate their reference method here

This is ^{15}N gas-flux method. This information will be added.

Line 159: Should also briefly mention what is the same treatment strategy employed in this study.

This is: identical fertilizer application procedure as fertilizer solution applied with needle injection technique, identical water and fertilizer addition and identical plots and chamber sizes. This information will be added.

Line 178: Why 20 mg N/kg of soil in lab incubation compared to 10 mg N/kg soil in field fertilisation?

This was wrongly described and will be corrected for: in both lab and field study total fertilization was 20 mg N per kg soil added as $NaNO_3$ (10 mg N) and NH_4Cl (10 mg N)).

Line 141: This is confusing. Why the dates for 'next field campaigns' do not correspond to what is written earlier?

These are dates when the cylinders were reinstalled, this was done at least one month before the next filed campaign. This will be clarified.

Line 217: How was N2O converted to N2? In-line conversion?

Yes, in-line reduction, this information will be added.

Line 298: nD is not included here. Why? Understand that the isotopic ranges are not very different between bD and nD but authors should briefly mention why this is not included here to avoid confusion. Also to show that the authors have considered the nD pathway as well.

nD cannot be really separated with this approach from bD. It will be clarified that the bD fraction here can possibly include nD as well.

Line 310: Why higher fungal DN compared to nitrification in this instance? The data in Table S2 can be used to briefly justify this?

We deal with rather high soil moisture, mostly over 65% WFPS, and also ammonium content was low, which rather favours fD than Ni. This explanation will be added.

Line 379: Some of the N2 fluxes are above the detection limit but the values written here are below the detection limit mentioned in line 373.

Sorry, this was a mistake, it is from 23 to 304 g N-N2. This will be corrected. Thank you for careful reading!

Line 421 - 423: Don't quite get what you mean here. Consider rephrasing. You mean corrected precursor ranges based on different fractionation factors?

It will be clarified. In this sentence one word was incorrectly used – precursors instead of endmembers. Sorry for this mistake.

Line 434: The minimum reduction line is not described in Fig. 1. The dotted lines and the mixing should be clearly described in the legend/caption.

This explanation will be added to the Fig.1 caption: The soild lines (bD-fD mixing and mean reduction line) are main assumptions used in the calculation procedures for SP/O Map. The grey dashed line shows the alternative bD-Ni mixing line (calculations with this alternative scenario are also presented in the supplement Table S2). The red dashed line shows the minimum reduction line – for the case of minimal delta values of the bD endmember. And for Fig.3 caption: The dashed line shows the linear fit for all the points with its equation and statistics above.

Line 461: There was relatively large discrepancy between lab and field NO3- and NH4+ values. In fact, the d15N-NH4+ is very heavy and the possible factors driving these values should be discussed.

We comment this in the discussion, L680: This indicates that the ammonium pool was highly fractionated and nearly exhausted. This is most probably due to adsorption processes. But this is just a speculation so far. The discussion on this issue will be extended in the follow up paper, where we also include the 15N-NH4 treatment which was not presented here. This information will be added in the manuscript.

Line 490: The authors mentioned that the high d15N-NH4+ has shifted the location of the nD and Ni in the end member mixing plot. What is the author comparing the shift to?

Ccompared to cases when similar $\delta^{15}N_{NH4}$ and $\delta^{15}N_{NO3}$ values are determined or assumed – this will be clarified in the text.

Line 551: Amplitude for 3D1 model, case 1 is not always lower than the reference – at the start and towards the end of sampling, the amplitude is higher than the reference method. Any explanation on why this is the case?

I meant lower amplitude of the temporal changes, this will be clarified in the text. The uncertainty of each method mostly depend on the standard deviation of 4 repetitions of which each time sample consists.

Line 670: I agree with the authors that recalculation of the literature mixing endmember values is important but my question is what fractionation factors should be considered when correcting these values and how to evaluate that these corrected ranges are justified?

We can take the literature ranges for fractionation factors based on pure culture studies (we have presented the summarised values in Table S1, they are also summarised in the supplement to new perspective paper Yu et al., 2020 (https://onlinelibrary.wiley.com/doi/abs/10.1002/rcm.8858)) . These values can be also determined experimentally for the particular soil under study, at least for denitrification, but this is complex and time consuming. But importantly the literature fractionation factors for particular processes must be corrected with the substrate isotopic signatures, which should be determined for each soil study. The procedure of this correction is presented in Table S1. We have also extended the description of this correction and will move this whole paragraph to the methods section.

For the graphical presentation of dual isotope plots for sampling points always $\delta^{18}O$ and $\delta^{15}N$ values of emitted N_2O are plotted ($\delta^{18}O_{N2O}$, $\delta^{15}N_{N2O}$). But the precursors isotopic signatures ($\delta^{18}O_{H2O}$, $\delta^{15}N_{NO3-}$, $\delta^{15}N_{NH4+}$) are taken into account by respective correction of mixing endmembers isotopic ranges (see Table S1). The literature endmember ranges are given as isotope effects (ε) expressed in relation to particular precursor relevant for particular pathway, e.g. for $\delta^{18}O$ of bD the $\varepsilon_{N2O/H2O}$ is calculated by subtracting the precursor isotopic signature (δ_{H2O}) from the measured δ_{N2O} values:

$$\varepsilon_{N2O/precursor} = \delta_{N2O} - \delta_{precursor} \tag{11}$$

e.g. for $\delta^{18}O$ of bD: $\delta_{N2O} = 10$, $\delta_{H2O} = -9$; $\varepsilon_{N2O/H2O} = 19$

Afterwards, the literature isotope effects are corrected with the actually measured precursor values determined for the particular study ($\delta_{\text{actual precursor}}$) to determine the characteristic isotopic signature of N_2O emitted from the particular mixing endmember for this particular study conditions ($\delta_{\text{N2O, endmember}}$):

$$\delta_{\text{N2O\_endmember}} = \varepsilon_{\text{N2O/precursor}} + \delta_{\text{actual precursor}} \tag{12}$$

e.g. $\delta^{18}O$ of bD: $\varepsilon_{\text{N2O/H2O}} = 19$, $\delta_{\text{actual H2O}} = -6.4$, $\delta_{\text{N2O\_bD}} = 12.6$.

Hence, the endmember ranges represent the expected isotopic signatures of N_2O originating from each mixing endmember for the particular case study characterised by specific precursor isotopic signatures. Such approach allows for presenting all data in the common isotopic scales without presumption on the dominating pathway and dominating precursor. Hence, this new approach presented here is actually a further development of Maps, since this allows for correcting both Ni and bD, fD and nD endmembers with relevant distinct precursors, in contrast to only correcting measured values with one common assumed precursor isotopic signature. In previous papers, where $\delta^{18}O$ and $\delta^{15}N$ related to precursors ($\delta^{18}O_{\text{N2O/H2O}}$, $\delta^{15}N_{\text{N2O/NO3}}$) were plotted (Ibraim et al., 2019; Lewicka-Szczebak et al., 2017; Lewicka-Szczebak et al., 2016) it was assumed that denitrification must be the dominating N_2O production pathway.

We will also move the Table 1 into the main manuscript, since it contains important information for these corrections.

Line 686: Be specific of what shift is meant here? Temporal?

Yes, temporal shift, this will be added.

Line 820: This sentence is rather subjective. Is it possible to provide a more definitive range here? Can the authors make use of a sensitivity analysis to show the extent of substrate isotopic variations effects on the accuracy of the mapping approach?

This is quite a complex analysis – it has been done for SP/O Map (Wu et al., 2019 https://www.sciencedirect.com/science/article/abs/pii/S0013935119306036) but not yet for isotope Maps applying d15N. This is definitely the topic for the further work and it is planned to be done soon. Without a precise analysis it is not possible to provide a precise numbers here.

Line 825: Can the author suggest the lowest N2O fluxes without compromising the precision of isotope maps and the 2DI model? This will be helpful as a guideline for future studies wanting to use these approaches.

Based on our F1 and F2 field case studies we can say that where N_2O flux was mostly below 10 $gN-N_2O$ $ha^{-1}d^{-1}$ the pathways partitioning was biased. This information will be added in the text.

N₂O isotope approaches for source partitioning of N₂O production and estimation of N₂O reduction – validation with ¹⁵N gas-flux method in laboratory and field studies

Dominika Lewicka-Szczebak[1,2], Maciej Piotr Lewicki[2,3] and Reinhard Well[3,4]

5   [1] Centre for Stable Isotope Research and Analysis, University of Göttingen, Büsgenweg 2, 37077 Göttingen, Germany
[2] Institute of Geological Sciences, University of Wrocław, pl. M. Borna 9, 50-204 Wrocław, Poland
[2,3] Institute of Theoretical Physics, University of Wrocław, pl. M. Borna 9, 50-204 Wrocław, Poland
[3,4] Thünen-Institut of Climate-Smart Agriculture, Bundesallee 50, 38116 Braunschweig, Germany

10   *Correspondence to*: Dominika Lewicka-Szczebak (dominika.lewicka@uni-goettingen.de)

Abstract.

The approaches based on natural abundance N₂O stable isotopes are often applied for the estimation of mixing proportions between various N₂O producing pathways as well as for estimation of the extent of N₂O reduction to
15   N₂. But such applications are associated with numerous uncertainties and hence their limited accuracy needs to be considered . Here we present the first systematic validation of these methods for laboratory and field studies applying the ¹⁵N gas-flux method as the reference approach.
Besides applying dual isotope plots for interpretation of N₂O isotopic data, for the first time we propose a three dimensional N₂O isotopocule model based on Bayesian statistics to estimate the N₂O mixing proportions and
20   reduction extent based simultaneously on three N₂O isotopic signatures (δ^{15}N, δ^{15}N^{SP} and δ^{18}O). Determination of mixing proportions of individual pathways with N₂O isotopic approaches appears often imprecise, mainly due to imperfect isotopic separation of the particular pathways. Nevertheless, the estimation of N₂O reduction is much more robust, when applying optimal calculation strategy, reaching typically accuracy of N₂O residual fraction determination of about 0.15.

1. Introduction

Nitrous oxide (N_2O) emission from soils and waters may result from numerous nitrogen transformation processes, mainly heterotrophic bacterial denitrification (bD), autotrophic nitrification (Ni), nitrifier denitrification (nD), and fungal denitrification (fD), but also heterotrophic nitrification, chemodenitrification, or co-denitrification (Butterbach-Bahl et al., 2013; Firestone and Davidson, 1989; Müller et al., 2014). The ability to distinguish the proportional contributions of these various N_2O origins (f_{bD}, f_{Ni}, f_{nD}, f_{fD}) is important ~~in~~ for constraining the N budget and ~~in~~ for developing and assessing the performance of mitigation strategies for N_2O emission, which significantly contributes to global warming and stratospheric ozone depletion (IPCC, 2007; Ravishankara et al., 2009). ~~Partition~~ Determination of the mixing proportions f_{bD}, f_{Ni}, and f_{nD} is only partially possible by combination of numerous experimental techniques, including sophisticated ^{15}N and ^{18}O isotope labelling techniques (Müller et al., 2014; Wrage-Mönnig et al., 2018). However, also natural abundance N_2O isotopic analyses have been often applied to estimate the possible proportional contribution of particular pathways (Toyoda et al., 2017; Yu et al., 2020) and are currently the only isotopic approach to identify f_{fD} (Rohe et al., 2017; Wrage-Mönnig et al., 2018). The ~~partition~~ determination of mixing proportions based on natural abundance N_2O isotopes is theoretically possible thanks to characteristic isotopic fractionation for each pathway, determined in numerous laboratory pure culture experiments (Toyoda et al., 2017), but practically very complex, mainly due to changes of N_2O isotopic signature during its partial reduction to N_2 and due to overlapping isotopic endmember values of individual pathways. N_2O isotopic analyses comprise the isotopic determination of: oxygen ($\delta^{18}O$), bulk nitrogen ($\delta^{15}N$) and nitrogen site preference ($\delta^{15}N^{SP}$), i.e., the difference in $\delta^{15}N$ between the central and the peripheral N atom of the linear N_2O molecules (Brenninkmeijer and Röckmann, 1999; Toyoda and Yoshida, 1999). All these three isotopic signatures ($\delta^{18}O$, $\delta^{15}N$ and $\delta^{15}N^{SP}$) show characteristic ranges of isotopic signatures for particular N_2O production pathways but are also altered during the N_2O reduction process.

N_2O reduction to N_2 occurs during the last step of microbial denitrification, i.e., anoxic reduction of nitrate (NO_3^-) to N_2 through the following intermediates: $NO_3^- \rightarrow NO_2^- \rightarrow NO \rightarrow N_2O \rightarrow N_2$ (Firestone and Davidson, 1989; Knowles, 1982). Commonly applied experimental techniques enable us to quantitatively analyse only the intermediate product of this process, N_2O, but not the final product, N_2 (Groffman, 2012; Groffman et al., 2006). This is due to the high atmospheric N_2 background precluding direct measurements of N_2 emissions in presence of the natural atmosphere (Bouwman et al., 2013; Saggar et al., 2013). Estimation of N_2-flux is possible with sophisticated laboratory experiments applying N_2-free helium atmosphere (Scholefield et al., 1997) or ^{15}N gas-flux method, i.e. ^{15}N analyses of gas fluxes after addition of ^{15}N-labelled substrate (Bergsma et al., 2001; Schmidt et al., 1998). Previous studies documented large possible variations in N_2 flux, and consequently also in the residual unreduced N_2O fraction: $r_{N2O} = y_{N2O}/(y_{N2}+y_{N2O})$ (y: mole fraction). In laboratory studies, the whole

scale of possible r_{N2O} variations, ranging from 0 to 1, had been found (Lewicka-Szczebak et al., 2017; Lewicka-Szczebak et al., 2015; Mathieu et al., 2006; Morse and Bernhardt, 2013; Senbayram et al., 2012). Due to technical limitations, so far only the ^{15}N gas-flux method had been applied in field conditions to determine r_{N2O} (Aulakh et al., 1991; Baily et al., 2012; Bergsma et al., 2001; Buchen et al., 2016; Decock and Six, 2013; Kulkarni et al., 2013; Mosier et al., 1986). Moreover, first attempt to apply the ^{15}N gas-flux method under N_2-reduced atmosphere in field has been presented recently (Well et al., 2019a). This new approach increases the sensitivity of ^{15}N gas-flux method (80-fold better sensitivity for N_2+N_2O flux measurements (Well et al., 2019a)) which was so far very limiting for successful application in field studies (Buchen et al., 2016). But still, application of this approach is technically very demanding and applicable only with a low temporal and spatial resolution. Hence, no comprehensive data sets from field-based measurements of soil N_2 emissions are available and this important component in soil nitrogen budget is still missing. This constitutes a serious shortcoming in understanding and mitigating the microbial consumption of nitrogen fertilisers (Bouwman et al., 2013; Seitzinger, 2008), and the N_2O ~~emission~~budget.

An alternative approach for assessing N_2 fluxes is the use of N_2O isotopes, which allows to indirectly determine r_{N2O} from ~~its~~ the isotopic signature of the residual N_2O (Ostrom et al., 2007; Well and Flessa, 2009), since the ~~magnitude of the observed isotope effect~~ increase in $\delta^{18}O$, $\delta^{15}N$ and $\delta^{15}N^{SP}$ of the residual N_2O due to N_2O reduction~~,~~ ~~depends largely on~~is related to r_{N2O} (Jinuntuya-Nortman et al., 2008; Menyailo and Hungate, 2006; Ostrom et al., 2007; Well and Flessa, 2009). This approach is also potentially applicable for quantification of r_{N2O} in field conditions (Buchen et al., 2018; Park et al., 2011; Toyoda et al., 2011; Verhoeven et al., 2019; Zou et al., 2014). Its advantage over the ^{15}N gas-flux method lies in its easier and non-invasive application, no need of additional fertilization, and much lower costs. But on the other hand, complexity of the N_2O production pathways with co-occurring N_2O reduction~~,~~ ~~and~~ variability of isotope effects and isotope fractionation associated with diffusion processes can make this estimation imprecise (Lewicka-Szczebak et al., 2015; Lewicka-Szczebak et al., 2014; Yu et al., 2020) ~~(Lewicka-Szczebak et al., 2015; Lewicka-Szczebak et al., 2014; Müller et al., 2014; Wu et al., 2019)~~. Since mostly two processes, mixing and reduction, determine the final N_2O isotopic signature, we need at least two isotopic values to be able to asses both: N_2O mixing ~~ratio~~proportions of ~~between~~ two N_2O production pathways and r_{N2O}. Therefore, often applied are the dual isotope plots, also called isotope Mapping approach (Map), *i.e.*, isotopic relations in the space $\delta^{15}N^{SP}/\delta^{15}N$ (SP/N Map) and $\delta^{15}N^{SP}/\delta^{18}O$ (SP/O Map). The SP/N Map has been first applied for agricultural soils by Toyoda et al. (2011). Afterwards many studies utilized this relation to determine N_2O mixing proportions and N_2O reduction (Kato et al., 2013; Wolf et al., 2015; Zou et al., 2014). Later, it was shown that $\delta^{18}O$ can be also used as a good tracer for N_2O production processes, thanks to high O-exchange during bD resulting in quite stable $\delta^{18}O$ values for this pathway (Lewicka-Szczebak et al., 2016). Based on this finding the SP/O Map for N_2O interpretation was proposed (Lewicka-Szczebak et al., 2017) and applied in recent studies (Buchen et al., 2018; Ibraim et al., 2019;

Verhoeven et al., 2019; Wu et al., 2019). Both SP/N and SP/O Map have been applied jointly for field studies (Ibraim et al., 2019) and showed quite a good agreement in the calculated r_{N2O} and f_{bD} values. However, so far these two approaches were not combined together into a complex three-dimensional model allowing the calculation of pathways mixing proportions and r_{N2O} based on three isotopic signatures ($\delta^{15}N$, $\delta^{18}O$, $\delta^{15}N^{SP}$) simultaneously. Development of such a model is a clear current need.

Precise quantification of both, the production pathway proportions and the extent of N_2O reduction with isotope Maps is limited by wide ranges of isotopic signatures reported for individual pathways, the overlapping of these isotopic signatures ranges, variations in substrate isotopic compositions, and variability of fractionation factors associated with N_2O reduction (Toyoda et al., 2017; Yu et al., 2020). Hence, it can be questioned how far we can trust the quantitative results provided by calculations based on isotope Maps. To answer this question comparisons with estimates based on independent methods are needed. The first attempt for comparing r_{N2O} obtained with SP/O Map and ^{15}N gas-flux method in a field case study was performed by Buchen et al. (2018). Due to non-identical treatment (different fertilizer application procedures: needle injection of fertilizer solution for ^{15}N treatments and surface distribution of fertilizer in NA treatments; different sizes of ^{15}N and NA microplots and chambers) and the consequent differences in soil moisture and mineral N, the results of both treatments were difficult to compare, however, the r_{N2O} values obtained indicated clearly the dominance of N_2 flux over N_2O flux by both methods. That study also presented analysis of various calculation scenarios applying upper and lower limits for mixing isotopic endmembers values and reduction fractionation factors, which revealed pronounced uncertainty of this calculation approach (Buchen et al., 2018). It was suggested that a further study on validation and uncertainty analysis of the SP/O Map is required with particular attention to identical treatment for both approaches under comparison. Another comparison was performed with archival datasets applying helium incubations as reference method and indicated large uncertainties of the calculations based on the SP/O Map (Wu et al., 2019). The huge uncertainties determined in these studies resulted from the fact that the full range of endmember values and fractionation factors reported in the literature was taken into account. But for particular soils and experimental conditions these ranges might be smaller and uncertainties thus lower. Hence, it is still unsure to which extent the ranges of isotopic fractionation factors determined in laboratory conditions and for pure culture studies are valid for particular experiments. It is not feasible to validate each isotope characteristic separately in field studies, since the pathways are not easily separable and this can be only achieved in controlled laboratory conditions.

While these recent studies indicated severe imprecision associated with the r_{N2O} estimations based on N_2O isotopocule approaches (Buchen et al., 2018; Wu et al., 2019), the suitability of this approach in estimation of r_{N2O} and mixing proportions has never been validated in a systematic study with a reference method. Hence, the idea of this study is to validate the methods based on N_2O isotope Maps and determine their attainable precision by parallel application with the reference method - ^{15}N gas-flux method. We compare the calculated N_2 flux

4

based on the ^{15}N gas-flux method (^{15}N treatment) and N_2O isotope Maps (natural abundance (NA) treatment) in laboratory and field experiments applying identical treatment strategy (meaning identical fertilizer application procedure: fertilizer solution applied with needle injection technique, identical water and fertilizer addition and identical plots and chamber sizes). Moreover, we present a new three-dimensional isotopocule model (3DI model) based on 3D isotopocule space and provide a validation of its outputs. This is the first attempt to systematically validate the results from N_2O natural abundance isotopic studies (N_2O isotopocule approaches) in laboratory and field conditions.

Our aim is to (1) validate applicability of N_2O isotopocule approaches for N_2 flux determination, (2) validate applicability of N_2O isotopocule approaches for partition of N_2O producing pathways and (3) to develop best evaluation strategy for interpretation of N_2O isotopic data.

2 Methods

2.1 Field study

Silt loam soil *Albic Luvisol* from arable cropland of Merklingsen experimental station located near Soest (North Rhine-Westphalia, Germany, 51°34'15.5"N, 8°00'06.8"E) was used (87% silt, 11% clay, 2% sand). The soil density of intact cores was 1.3 g ml^{-1}, pH value 6.8, total C content 1.30%, total N content 0.16%, organic matter content 2.14%. The field was sown with winter rye in September 2015 and mineral under foot fertilization was applied. Our experiments were conducted on experimental plots of a field study on management effects on greenhouse gas fluxes. We selected the 'climate-optimized farm' treatment where a complex cropping rotation of silage maize - winter wheat - faba bean – winter barley – perennial rye had been established since 2010 (Kramps-Alpmann et al., 2017). This treatment was managed by zero-tillage with direct seeding and ~~fertilisation~~fertilization was a combination of organic (biogas digestate) and mineral fertilizer where doses were set according to official fertilizer recommendations (Baumgärtel and Benke, 2009). On 13th October in each of the four replicate plots (6 * 12 m) we established microplots consisting of aluminum cylinders (length 35cm, diameter 15cm) inserted to 30cm depth into the soil so that 5cm extended above the ground for installation of the flux chamber. Three field campaigns were carried out in November 2015 (F1), March 2016 (F2) and Mai/June 2016 (F3). After each field campaign the cylinders were removed, cleaned and later reinstalled on new locations ~~for the next field campaign~~ (on 27 Nov 2015 for F2 sampling and on 28 April 2016 for F3 sampling)~~.~~ for the next field campaign.

On each replicate plot cylinders were installed pairwise – one for gas flux measurements and one for mineral nitrogen sampling – for 3 treatments – natural abundance (NA), traced nitrate ([15]NO_3^-) and traced ammonium ([15]NH_4^+) – in total 6 cylinders per replicate plot. The distance between each treatment cylinder was at least 2m, pair of cylinders for one treatment were in 0.5m distance.

At the beginning of the experiment, a fertilizer solution with 240 mg N L^{-1} as NaNO$_3$ and 240 mg N L^{-1} as NH$_4$Cl was added to the experimental microplots through needle injection technique. Three mL of the fertilizer solution was injected into 72 points using 12 needles inserted subsequently into 6 depths (2.5 - 7.5 - 12.5 - 17.5 - 22.5 - 27.5 cm) from the top to the bottom using peristaltic pump. This strategy was based on previous studies (Buchen et al., 2016; Wu et al., 2011) and was enhanced by pre-experimental tests to obtain the most homogeneous tracer distribution (Lewicka-Szczebak and Well, 2020). Total fertilization was 20 mg N per kg soil (added as NaNO$_3$ (10 mg N) and NH$_4$Cl (10 mg N)) ~~10 mg N per kg soil~~ which was equivalent to about ~~40~~ 80 kg N per ha.

In total, 216 mL of fertilizing solution was inserted into each microplot which resulted in 3 % increase in water content. For ^{15}N-labelled treatments the ^{15}N content in fertilizing solution was calculated to achieve about 60 atom % ^{15}N in the ^{15}N-labelled N pool. The ^{15}NO$_3^-$ treatment received tracer solution containing 68 atom % ^{15}N and the ^{15}NH$_4^+$ treatment received 64 atom % ^{15}N.

Immediately after fertilizing solution addition, the flux chamber microplots were closed for gas accumulation. Opaque PVC chambers of an area of 1.767 dm^2 and a volume of 2.65 dm^3 were applied with installed valves for sample collection and a fan for gas mixing. The closed chamber method (Hutchinson and Mosier, 1981) was used for N$_2$O flux measurement. Chambers were closed and sealed with air-tight rubber bands for 120 min and headspace sampling was performed after 40, 80 and 120 min into evacuated crimped 20 mL vials with a 30 mL syringe for gas-flux measurements. Additionally, after 120 min, samples for isotope analysis were collected. For ^{15}N treatments two identical replicates were taken into 12 mL evacuated screw-cup Exetainers® (Labco Limited, Ceredigion, UK) with two combined 15 mL syringes. For the NA treatment, one gas sample was transferred into an evacuated 115 mL crimp-cap vial with a 150 mL syringe.

Each field campaign lasted 5 days. Gas samples were collected once on the first day after fertilization, afterwards twice a day – in the morning and in the evening, and once on the last 5th day in the morning.

The soil sampling microplots were treated identically and used for mineral nitrogen sampling. The soil samples were collected with a Goettinger boring rod with 18 mm outer diameter and 14 mm slots (Nietfeld GmbH, Quakenbrück, Germany). Boreholes were sealed by inserting a closed sand-filled PVC pipe with the same diameter as the bore. For each sampling, three cores were collected and homogenised to one mixed sample each day, hence we performed 5 soil samplings during each campaign. The samples were immediately transported to the laboratory at 6°C and mineral nitrogen extractions were performed on the same day.

2.2 Laboratory incubation

The soil from the experimental field site was used to prepare incubation columns for laboratory incubation. The soil, upper 30cm layer, was collected on the 18.01.2018 from the experimental plot used previously for field campaigns and the incubation was conducted from 19.02.2018 to 05.03.2018. The soil was air dried and sieved

at 4 mm mesh size. Afterwards, the soil was rewetted to achieve- a water content equivalent to 60 % water-filled pore space (WFPS) and fertilised with 20 mg N per kg soil, added as $NaNO_3$ (10 mg N) and NH_4Cl (10 mg N). Analogically as in the field study, three treatments were prepared: natural abundance (NA), labelled with ^{15}N nitrate ($^{15}NO_3$) and labelled with ^{15}N ammonium ($^{15}NH_4$). For the $^{15}NO_3$ treatment, $NaNO_3$ solution with 72 atom % ^{15}N was added and for the $^{15}NH_4$ treatment, NH_4Cl solution with 63 atom % ^{15}N was added. Then soils were thoroughly mixed to obtain homogenous distribution of water and fertilizer and an equivalent of 1.69 kg dry soil was repacked into each incubation column with bulk density of 1.3 g cm^{-3}.

For each treatment 14 columns were prepared, and half of them received additional water injected on the top of the column (100 mL water added) to prepare two moisture treatments: dry (61 % WFPS) and wet (72 % WFPS). The incubation lasted 12 days. In the meantime, on the 6th day of incubation, water addition on the top of each column was repeated (80 mL water added) to increase the soil moisture in both treatments to ca. 68 % WFPS in the dry treatment and ca. 81 % WFPS in the wet treatment. The WFPS values were controlled during the experiment (Fig. S1). -The strategy of adding water on the top of the column to achieve target water content was necessary to allow mixing and compaction at a suitable (low) water content of the soil and thus to optimise homogeneity of water and fertilizer distribution (Lewicka-Szczebak and Well, 2020). The incubation temperature was 20°C. The columns were continuously flushed with a gas mixture with reduced N_2 content to increase the measurements sensitivity (2% N_2 and 21% O_2 in He, (Lewicka-Szczebak et al., 2017)) with a flow of 9 mL min^{-1}. Gas samples were collected daily into two 12 mL septum-capped Exetainers® (Labco Limited, Ceredigion, UK) and one crimped 100 mL vial connected to the vents of the incubation columns. Soil samples were collected 5 times during the incubation by sacrificing one incubation column per sampling event, which was then divided into three subsamples (replicate samples of mixed soil).

2.3 Gas analyses

Measurements of N_2O concentrations in the 20 mL samples were carried out with a gas chromatograph (GC, 2014; Shimadzu, Duisburg, Germany) equipped with an electron capture detector (ECD) and an autosampler (Loftfields Analytical Solutions, Neu Eichenberg, Germany). The analytical precision was around 2%.

Flux rates of total N_2O for field campaigns, *i.e.*, including fluxes from ^{15}N-labelled and non-labelled sources, were calculated from ordinary linear regression of the four consecutive samples over time using the R package gasfluxes (Fuß, 2015) and the following equation:

$$J_{N2O} = \frac{dc_{N2O}}{dt} * \frac{V}{A} \tag{1}$$

where J_{N2O} is the flux rate in µg N_2O-N m^{-2} h^{-1}, C_{N2O} is N_2O mass concentration in µg N m^{-3} corrected by the chamber temperature according to the ideal gas law, t is closing time of the chamber, V is volume of the chamber in m^3 and A is covered soil area in m^2.

For laboratory incubations fluxes were calculated based on the dynamic chamber principle. Correction for the inlet concentration is omitted since the N_2O-free gas mixture was used for flushing ~~due to constant flow~~ through the following equation was applied:

$$J_{N2O} = C_{N2O} * \frac{Q}{A} \tag{2}$$

where J_{N2O} is the flux rate in µg N_2O-N m^{-2} h^{-1}, C is N_2O mass concentration in µg N m^{-3} corrected by the incubation temperature according to the ideal gas law, Q is the gas flow rate through the incubation vessels in m^3 h^{-1}, and A is soil area in the incubation vessel in m^2.

The gas samples collected from ^{15}N treatments were analyzed for ^{15}N content with a modified GasBench II preparation system coupled to MAT 253 isotope ratio mass spectrometer (Thermo Scientific, Bremen, Germany) according to Lewicka-Szczebak et al. (2013). In this set-up, N_2O is converted to N_2 during in-line reduction~~prior to analysis, which allows simultaneous measurement of~~and stable isotope ratios ^{29}R (^{29}N$_2$/^{28}N$_2$) and ^{30}R (^{30}N$_2$/^{29}N$_2$), of N_2, of the sum of denitrification products (N_2+N_2O) and of N_2O are determined. Based on these measurements the following values are calculated according to the respective equations (after Spott et al. (2006)):

The ^{15}N abundance of ^{15}N-labelled pool (a_P) from which N_2 (a_{P_N2}) or N_2O (a_{P_N2O}) originate is calculated as follows:

$$a_P = \frac{^{30}x_M - a_M \cdot a_{bgd}}{a_M - a_{bgd}} \tag{3}$$

The calculation of a_P is based on the non-random distribution of N_2 and N_2O isotopologues (Spott et al., 2006) where $^{30}x_M$ is the fraction of ^{30}N$_2$ in the total gas mixture:

$$^{30}x_M = \frac{^{30}R}{1 + ^{29}R + ^{30}R} \tag{4}$$

a_M is ^{15}N abundance in total gas mixture

$$a_M = \frac{^{29}R + 2\,^{30}R}{2(1 + ^{29}R + ^{30}R)} \tag{5}$$

a_{bgd} is ^{15}N abundance of non-labelled pool (atmospheric background or experimental matrix)

The fraction originating from the ^{15}N-labelled pool (f_P) for N_2 (f_{P_N2}), N_2+N_2O (f_{P_N2+N2O}) and N_2O (f_{P_N2O}) within the total N of the sample is calculated as follows:

$$f_P = \frac{a_M - a_{bgd}}{a_P - a_{bgd}} \tag{6}$$

8

The fraction originating from the ^{15}N-labelled pool within the sample (f_{N2}) is calculated, taking into account the actual N_2 concentration background in the sample C_{N2}:

$$f_{N2} = f_{P\_N2} * C_{N2} \tag{7}$$

From the f_{N2} value determined with Eq.7 the N_2 flux was calculated, in the same manner as for N_2O, for field campaigns (Eq. 1):

$$J_{N2} = \frac{f_{N2}}{dt} * \frac{V}{A} \tag{8}$$

where J_{N2} is the N_2 flux rate in µg N_2-N m^2 h^{-1}, f_{N2} is N_2 mass concentration in µg N m^3 corrected by the chamber temperature according to the ideal gas law, t is closing time of the chamber, V is volume of the chamber in m^3 and A is covered soil area in m^2. Chamber closing time was 120 min and for one chosen field study (F3) the linearity of N_2 increase over 120 min was checked and confirmed. The fluxes correction for underestimation due to subsoil flux and gas soil storage (Well et al., 2019b) was not performed because the focus of this paper was to determine r_{N2O} while subsoil diffusion of N_2 and N_2O is almost identical. This correction would thus not significantly impact r_{N2O}. But the fluxes shown in Fig. S2 are measured fluxes and include the underestimation of ^{15}N-based estimates (Well et al., 2019b).

For laboratory incubations with the constant flow through N_2 flux was determined in the same manner as respectively for N_2O (Eq. 2):

$$J_{N2} = f_{N2} * \frac{Q}{A} \tag{9}$$

where J_{N2} is the N_2 flux rate in µg N_2-N m^{-2} h^{-1}, f_{P_N2} is N_2 mass concentration in µg N m^3 corrected by the chamber temperature according to the ideal gas law, Q is the gas flow rate through the incubation vessels in m^3 h^{-1}, and A is soil area in the incubation vessel in m^2.

N_2O residual fraction (r_{N2O}) representing the unreduced N_2O mole fraction of total gross N_2O production (Lewicka-Szczebak et al., 2017) is calculated as:

$$r_{N2O} = \frac{J_{N2O}}{J_{N2O} + J_{N2}} \tag{10}$$

where J_{N2O} and J_{N2} are the N_2O and N_2 flux rates in µg N_2O-N m^{-2} h^{-1}.

The analytical detection limit of the calculated N_2 flux from the ^{15}N labelled pool was approx. 50 µg N m^2 h^{-1} for field studies and approx. 1.5 µg N m^2 h^{-1} for laboratory experiments (due to increased sensitivity as a result of the N_2-reduced atmosphere).

The gas samples collected in NA treatments were analyzed for isotopocule N_2O signatures using a Delta V isotope ratio mass spectrometer (Thermo Scientific, Bremen, Germany), coupled to an automatic preparation system with Precon + Trace GC Isolink (Thermo Scientific), where N_2O was pre-concentrated, separated and purified and m/z 44, 45, and 46 of the intact N_2O^+ ions as well as m/z 30 and 31 of NO^+ fragment ions were determined. The results were evaluated accordingly (Röckmann et al., 2003; Toyoda and Yoshida, 1999;

Westley et al., 2007) which allows the determination of average $\delta^{15}N$, $\delta^{15}N^{\alpha}$ ($\delta^{15}N$ of the central N position of the N$_2$O molecule), and $\delta^{18}O$. $\delta^{15}N^{\beta}$ ($\delta^{15}N$ of the peripheral N position of the N$_2$O molecule) was calculated as $\delta^{15}N$ =($\delta^{15}N^{\alpha}$ + $\delta^{15}N^{\beta}$)/2 and ^{15}N site preference ($\delta^{15}N^{SP}$) as $\delta^{15}N^{SP}$ = $\delta^{15}N^{\alpha}$ - $\delta^{15}N^{\beta}$.

Pure N$_2$O analysed for isotopocule values in the laboratory of the Tokyo Institute of Technology was used as internal reference gas applying calibration procedures reported previously (Toyoda and Yoshida, 1999; Westley et al., 2007). Moreover, the standards from a laboratory inter-comparison (REF1, REF2) were used for performing two-point calibration for $\delta^{15}N^{SP}$ values (Mohn et al., 2014). All isotopic values are expressed as ‰ deviation from the $^{15}N/^{14}N$ and $^{18}O/^{16}O$ ratios of the reference materials (i.e. atmospheric N$_2$ and Vienna Standard Mean Ocean Water (VSMOW), respectively). The analytical precision determined as standard deviation (1σ) of the internal standards for measurements of $\delta^{15}N$, $\delta^{18}O$, and $\delta^{15}N^{SP}$ was typically 0.1, 0.1, and 0.5 ‰, respectively.

2.4 Soil analyses

All soil samples were homogenized. Soil water content was determined by weight loss after 24 h drying in 110ºC. Soil pH was determined in 0.01 mol CaCl$_2$ solution (ratio 1:5). Nitrate and ammonium concentration was determined by extraction in 2M KCl in 1:4 ratio by 1h shaking. Nitrite concentration was determined in alkaline extraction solution of 2M KCl with addition of 2M KOH (25 mL per L) in 1:1 ratio for 1 minute of intensive shaking (Stevens and Laughlin, 1995). The amount of added KOH was adjusted to keep the alkaline conditions in extracts (pH over 8). After shaking, the samples were centrifuged for 5 minutes and filtrated. The extracts for NO$_2^-$ measurements were stored at -4 °C and analyzed within 5 days. NO$_3^-$, NH$_4^+$ and NO$_2^-$ concentrations were determined colorimetrically with an automated analyser (Skalar Analytical B.V., Breda, the Netherlands).

To determine isotopic signatures of mineral nitrogen in NA treatments, microbial analytical methods were applied. For nitrate, the bacterial denitrification method with *Pseudomonas aureofaciens* was applied (Casciotti et al., 2002; Sigman et al., 2001). For nitrite, the bacterial denitrification method for selective nitrite reduction with *Stenotrophomonas nitritireducens* was applied (Böhlke et al., 2007), also for ^{15}N-enriched samples from ^{15}N treatments. For ammonium, a chemical conversion to nitrite with hypobromite oxidation (Zhang et al., 2007) followed by bacterial conversion of nitrite after pH adjustment was applied (Felix et al., 2013).

In ^{15}N treatments, ^{15}N abundances of NO$_3^-$ (a_{NO3-}) and NH$_4^+$ (a_{NH4+}) were measured according to the procedure described in Stange et al. (2007) and Eschenbach et al. (2017). NO$_3^-$ was reduced to NO by Vanadium-III chloride (VCl$_3$) and NH$_4^+$ was oxidized to N$_2$ by hypobromite (NaOBr). NO and N$_2$ were used as measurement gas. Measurements were performed with a quadrupole mass spectrometer (GAM 200, InProcess, Bremen, Germany).

2.5 N₂O isotope mapping approach (Map)

The Mapping approach is based on the different slopes of the mixing line between bD (possibly including also nD) and fD or Ni and the reduction line reflecting isotopic enrichment of residual N₂O due to its partial reduction in dual isotope plots. Both lines are defined from the known most relevant literature data on the respective mixing endmembers isotopic signatures and reduction fractionation factors. The detailed isotopic characteristics applied for the isotope Maps are presented in ~~the supplement (~~Table ~~S~~1~~)~~ and follow the most recent review paper (Yu et al., 2020). The detailed calculation strategy for SP/O Map can be found in the Supplement for the Wu et al. (2019) paper and for SP/N Map in the Supplement for the Toyoda et al. (2011) paper. The calculations are performed according to two possible cases of N₂O mixing and reduction:

- Case 1 - N₂O produced from bD is first partially reduced to N₂, followed by mixing of the residual N₂O with N₂O from other pathways,

- Case 2 - N₂O produced by various pathways is first mixed and afterwards reduced.

The calculations can be performed following different scenarios of particular endmember mixing: either bD-fD mixing or bD-Ni mixing. For our case studies, due to rather high soil moisture (>60% WFPS) and low ammonium content (Table 2), we rather expect higher fD contribution than Ni, hence the bD-fD mixing was applied and contribution of Ni was neglected. In the supplement, we also present a comparison of calculation results based on both mixing scenarios bD-fD and bD-Ni (Table ~~S2~~ S1 and supplementary spreadsheet table). This comparison only show pronounced differences for F1 treatment. nD cannot be separated from bD fraction in this approach due to isotope overlap (Fig.1), and the calculated bD fraction may also include nD.

For the graphical presentation of dual isotope plots for sampling points always $\delta^{18}O$ and $\delta^{15}N$ values of emitted N₂O are plotted ($\delta^{18}O_{N2O}$, $\delta^{15}N_{N2O}$). But the precursors isotopic signatures ($\delta^{18}O_{H2O}$, $\delta^{15}N_{NO3^-}$, $\delta^{15}N_{NH4^+}$) are taken into account by respective correction of mixing endmembers isotopic ranges (see Table 1). The literature endmember ranges are given as isotope effects (ε) expressed in relation to particular precursor relevant for particular pathway:

$$\varepsilon_{N2O/precursor} = \delta_{N2O} - \delta_{precursor} \tag{11}$$

e.g. for $\delta^{18}O$ of bD the $\varepsilon_{N2O/H2O}$ is calculated by subtracting the precursor isotopic signature (δ_{H2O}) from the measured δ_{N2O} values, i.e.: $\delta_{N2O} = 10$, $\delta_{H2O} = -9$; $\varepsilon_{N2O/H2O} = 19$

Afterwards, the literature isotope effects are corrected with the actually measured precursor values determined for the particular study ($\delta_{actual\ precursor}$) to determine the characteristic isotopic signature of N₂O emitted from the particular mixing endmember for this particular study conditions ($\delta_{N2O,\ endmember}$):

$$\delta_{N2O\ endmember} = \varepsilon_{N2O/precursor} + \delta_{actual\ precursor} \tag{12}$$

e.g. for $\delta^{18}O$ of bD: $\varepsilon_{N2O/H2O} = 19$, $\delta_{actual\ H2O} = -6.4$, $\delta_{N2O\ bD} = 12.6$.

Hence, the endmember ranges represent the expected isotopic signatures of N_2O originating from each mixing endmember for the particular case study characterised by specific precursor isotopic signatures. Such approach allows for presenting all data in the common isotopic scales without presumption on the dominating pathway and dominating precursor. Hence, this new approach presented here is actually a further development of Maps, since this allows for correcting both Ni/nD and bD/fD endmembers with relevant distinct precursors, in contrast to only correcting measured values with one common assumed precursor isotopic signature. In previous papers, where $\delta^{18}O$ and $\delta^{15}N$ related to precursors ($\delta^{18}O_{N2O/H2O}$, $\delta^{15}N_{N2O/NO3}$) were plotted (Ibraim et al., 2019; Lewicka-Szczebak et al., 2017; Lewicka-Szczebak et al., 2016) it was assumed that denitrification must be the dominating N_2O production pathway.

Table 1

2.6 Three-dimensional N_2O isotopocule model (3DI model)

The probability distributions of proportional contributions f_{-i} were determined using a stable isotope mixing model in the Bayesian framework. ~~(Parnell et al., 2013).~~ This allowed us to integrate three N_2O isotopic signatures into one model to find the nearest solution for the r_{N2O} and mixing proportions.

The core of the model was based on the work of Moore and Semmens (2008) which was further extended with implementation of N_2O reduction in two possible cases (analogically as for Map – see Section 2.5):

Case 1) $\qquad f_{bD}\left(\delta_{bD} + \varepsilon\, ln(r_{bD})\right) + f_{nD}\delta_{nD} + f_{fD}\delta_{fD} + f_{Ni}\delta_{Ni} = \delta_{N2O}$

$\qquad$ (~~11~~13)

Case 2) $\qquad f_{bD}\delta_{bD} + f_{nD}\delta_{nD} + f_{fD}\delta_{fD} + f_{Ni}\delta_{Ni} + \varepsilon\, ln(r_{N2O}) = \delta_{N2O}$

$\qquad$ (~~12~~14)

where f stands for fraction of N_2O originating from a particular pathway and δ stands for isotopic signature characteristic of this pathway, respectively for bD, nD, fD and nitrification Ni. ε is the isotope fractionation factor for N_2O reduction to N_2 and r_{N2O} is the N_2O residual fraction as defined in Eq. 10. r_{bD} is the N_2O residual fraction of bacterial denitrification only, as it is assumed in Case 1. This value can be recalculated to obtain r_{N2O} as follows:

$\qquad r_{N2O} = f_{bD}r_{bD} + f_{nD} + f_{fD} + f_{Ni}$

$\qquad$ (~~13~~15)

Let us briefly summarize the key assumptions and features of the statistical model. The input data of measured m isotope signatures (here three: $\delta^{15}N$, $\delta^{15}N^{SP}$, $\delta^{18}O$) from n sources (here four: bD, nD, fD and Ni) is assumed to be normally distributed and multiple measurements (here: 1 to 7 replicates) constitute a single sample, on which the Monte-Carlo integration is performed. The uncertainties of the source's data is fed into the model through the

variance in the calculation of unnormalized likelihood (see eq. ~~16~~18). For ~~P~~prior distributions of parameters ~~were assumed uninformative, i.e.,~~ flat Dirichlet distribution was used for proportional source contributions f ~~f_i~~ and uniform distribution for reduction parameter r. For each random sample ~~(f_i~~ f_i, r) a mean and a variance of each isotope signature j are calculated (different for two cases listed above):

Case 1) $\mu_j = \sum_{i=1}^{n}(f_i \delta_{ij}) + f_{bD}\, \varepsilon\, ln(r_{bD}), \sigma_j = \sqrt{\sum_{i=1}^{n}(f_i \sigma_{ij}^2) + f_{bD}\,|ln(r_{bD})|\sigma_{\varepsilon j}^2}$

(~~14~~16)

Case 2) $\mu_j = \sum_{i=1}^{n}(f_i \delta_{ij}) + \varepsilon\, ln(r_{N2O}), \sigma_j = \sqrt{\sum_{i=1}^{n}(f_i \sigma_{ij}^2) + |ln(r_{N2O})|\sigma_{\varepsilon j}^2}$

(~~15~~17)

and the likelihood of such a combination is calculated as:

$$L(x \mid \mu_j, \sigma_j) = \prod_{k}^{N} \prod_{j}^{m} \left[\frac{1}{\sigma_j \sqrt{2\pi}} exp\left(\frac{-(x_{kj}-\mu_j)^2}{2\sigma_j^2} \right) \right]$$

(~~16~~18)

where x ~~$_{kj}$~~ $_{kj}$ stands for k-th measurement of the sample and j-th isotope signature. We use the Markov-chain Monte-Carlo with the Metropolis condition: L ~~$_{(i+1)}$~~$/L$ ~~$_{(i)}$~~e ~~>=~~ $\geq \alpha$ ~~alpha~~, where alpha is a random variable sampled from a uniform distribution.

The detailed input parameters for the model are presented in ~~the supplement (~~Table S1~~)~~. The detailed isotopic characteristics to be applied for the isotope signatures of mixing endmembers and reduction fractionation factors are adopted after the most recent review paper (Yu et al., 2020).

2.7 Statistics

For results comparisons, an analysis of variance was used with the significance level α of 0.~~05~~1. The uncertainty values provided for the measured parameters represent the standard deviation (1σ) of the replicates. The propagated uncertainty was calculated using Gauss' error propagation equation taking into account standard deviations of all individual parameters.

The agreement with the reference method was assessed with the Nash–Sutcliffe efficiency (F) (Nash and Sutcliffe, 1970), which represent the R of the fit to the 1:1 line between observed reference (O) and estimated (E) values, as also used in previous validation studies (Lewicka-Szczebak et al., 2017; Wu et al., 2019):

$$F = 1 - \frac{\sum_{i=1}^{n}(O_i - E_i)^2}{\sum_{i=1}^{n}(O_i - O)^2}$$

(~~17~~19)

where E_i is the r_{N2O} value estimated with the method under validation, corresponding to the observed r_{N2O} value determined with the reference method: O_i, and O is the observed mean. In this assessment, an F=1 refers to a

perfect fit between estimated and reference values, lower F values indicate worse model fits, whereas a negative F occurs when the observed mean is a better predictor than the model.

3. Results

3.1 Soil properties

415 Soil organic N was analyzed in soil samples from each sampling campaign and varied only slightly with content of 0.141 ± 0.007 % N and isotopic signature $\delta^{15}N$ of 7.4 ± 0.4‰. $\delta^{18}O$ of soil water varied only slightly for field campaigns and equaled -6.7 ‰ for F1, -7.0 ‰ for F2, and -6.4 ‰ for F3, but was higher for incubation experiments with mean of -5.3 ‰. Detailed characteristics for mineral nitrogen contents and isotopic signatures are presented in Table ~~1~~2. The variations in water and nitrate content during the field campaigns and laboratory

420 incubations with comparison between NA and ^{15}N treatment are presented in the supplement (Fig. S1). Importantly, for vast majority of sampling points these soil conditions are well comparable between both treatments which allows for the methods comparison. Significant difference was only noted for nitrate content for the last sample in L2 and for water content for the last sample in F1 (Fig. S1).

3.2 Field campaigns

425 The first field campaign F1 in Nov 2015 (23rd Nov-27th Nov) showed low N_2O fluxes from 1.2 to 33.2 g N-N_2O ha^{-1}d^{-1} (Table ~~1~~2). N_2O isotopic signatures were determined for all the samples except one. The N_2 fluxes were under the detection limit for all samples, i.e. below 11 g N-N_2O ha^{-1} d^{-1}. In this case, the reference r_{N2O} values form the ^{15}N treatment could not be precisely determined. However, from the information that N_2 flux is below the detection limit even for the highest N_2O fluxes observed we can assess that r_{N2O} must be higher than 0.75.

430 For F1, soil temperature varied from 1.6 to 8.6 °C, mean 4.1 °C, WFPS varied from 54.1 to 72.4 %, mean 65 %. The second field campaign F2 in March 2016 (7th March-11th March) showed very variable N_2O fluxes from 0.5 to 110.7 g N-N_2O ha^{-1} d^{-1}. N_2O isotopic signatures could be determined only in 17 samples from 26. The N_2 fluxes were above the detection limit for 15 samples from 26, and varied from ~~1~~23 to ~~9~~304 g N-N_2O ha^{-1} d^{-1}. In this case, the reference r_{N2O} values form the ^{15}N treatment could be determined for 4 sampling dates out of 8. For

435 F2, soil temperature varied from 1.4 to 12.0 °C, mean 6.4 °C, WFPS varied from 57.9 to 77.9 %, mean 69 %. The third field campaign F3 in Mai/June 2016 (30th Mai-3rd June) showed very high N_2O fluxes from 1 to 1471 g N-N_2O ha^{-1}d^{-1}. N_2O isotopic signatures could be determined in all samples. The N_2 fluxes were always above the detection limit and varied from 114 to 2060 g N-N_2O ha^{-1} d^{-1}. In this case, the reference r_{N2O} values form the ^{15}N treatment could be determined for all 8 sampling times. For F3, soil temperature varied from 17.0 to 32.5 °C,

440 mean 21.4 °C, WFPS varied from 52.1 to 72.0 %, mean 62 %.

14

The detailed variations in gas fluxes during field campaigns and variations in ^{15}N abundance in various pools (a_{NO3}, a_{P_N2O} and a_{P_N2}) and the N_2O ^{15}N-pool derived fraction (f_{P-N2O}) are presented in the supplement (Fig. S2 C-E and Fig. S3 C-E). There are no significant differences in N_2O flux between ^{15}N and NA treatment (Fig. S2 C-E). In F3 the fluxes were much larger than in F1 and F2 and were decreasing during the sampling campaign, whereas N_2 flux was very variable and showed large differences between repetitions, represented by large error bars (Fig. S2 E). In F1 and F2 the ^{15}N-pool derived fraction was significantly lower when compared to F3. In F3 a_{P_N2} and a_{P_N2O} was comparable and higher than a_{NO3} in the first three samples and similar with a_{NO3} for the last 5 samples. In F2 a_{P_N2O} strictly depended on a_{NO3} and both showed clear decreasing trend, whereas a_{P_N2} was determined only in two sampling points and was significantly lower than a_{P_N2O} and a_{NO3}.

3.3 Laboratory experiments

The laboratory experiment L1 was conducted in dryer conditions than L2. In L1 initially WFPS was about 60 % and after water addition (9th day of the experiment) it was increased to 65%. In L2 initially WFPS was about 70 % and after water addition (9th day of the experiment) it was increased to 80 %.

N_2O fluxes in L1 were quite low from 0.2 to 16.7 g N-N_2O $ha^{-1}d^{-1}$. N_2O isotopic signatures could be determined in 38 from 56 samples. The N_2 fluxes were above the detection limit only for 43 from 112 samples and varied from 0 1.5 to 69.4 85 g N-N_2O $ha^{-1}d^{-1}$. In this case the reference r_{N2O} values form the ^{15}N treatment could only be determined for 7 sampling times out of 10. In L2 N_2O fluxes were higher and varied in wide range from 0.4 to 297.4 gN-N_2O $ha^{-1}d^{-1}$. N_2O isotopic signatures could be determined in 40 from 56 samples. The N_2 fluxes were above the detection limit only for 87 from 112 samples and varied from 1.2 0 to 199 g N-N_2O $ha^{-1}d^{-1}$. In this case, the reference r_{N2O} values form the ^{15}N treatment could be determined for 9 sampling times out of 10.

The detailed variations in gas fluxes during laboratory incubations and variations in ^{15}N abundance in various pools (a_{NO3}, a_{P_N2O} and a_{P_N2}) and the N_2O ^{15}N-pool derived fraction (f_{P-N2O}) are presented in the supplement (Fig. S2 A-B and Fig. S3 A-B). We often observe significantly different fluxes for NA and ^{15}N treatment: for L1 only for 2 samples (4 and 5) NA treatment show significantly higher N_2O flux but for L2 majority of sampling points show significantly higher N_2O flux in ^{15}N treatment, particularly for the last 4 sampling points, after the water addition (Fig. S2 B). Importantly, water content did not differ for this sampling points. In L1 the ^{15}N-pool derived fraction was significantly lower when compared to L2. In both L1 and L2 a_{P_N2}, a_{P_N2O} and a_{NO3} show comparable ranges and only very slight decreasing trend (Fig. S3 A-B).

Table 1 2 Results summary

15

3.5 Maps

~~In previous papers, where $\delta^{18}O$ and $\delta^{15}N$ related to precursors ($\delta^{18}O_{N2O/H2O}$, $\delta^{15}N_{N2O/NO3}$) were plotted (Ibraim et al., 2019; Lewicka Szczebak et al., 2017; Lewicka Szczebak et al., 2016) it was assumed that denitrification must be the dominating N$_2$O production pathway.~~

SP/O Map

Fig. 1

The majority of isotope results presented in the SP/O Map (Fig.1) is situated within the area limited by reduction and mixing lines, which allows for application of the calculation approach based on SP/O Map. Numerous samples, mostly from the laboratory incubation studies, are situated below the mean reduction line but within the minimum reduction line. For these samples, the calculation results provide f_{bD} values slightly above 1, which are set for 1 for the further summaries. All calculations and results can be followed in the spreadsheet file in supplementary materials.

The endmembers isotope values applied here (after Yu et al. (2020)) differ for nitrification $\delta^{18}O$ when compared to previous applications of SP/O Map (Buchen et al., 2018; Ibraim et al., 2019; Lewicka-Szczebak et al., 2017; Verhoeven et al., 2019). The currently applied $\delta^{18}O$ endmember values for Ni (23.5 ± 2.1‰) are lower than previously applied range (from 38.0 to 55.2 ‰, mean 43.0 ‰) and thus result in a separation of Ni and fD, which was not possible in the previous studies. With the current values, we have two possible mixing lines (bD-Ni and bD-fD), whereas in previous studies only one mixing line was applied (bD-(Ni+fD)). This requires the choice of most appropriate mixing scenario for the particular case study. For this study, the results obtained for r_{N2O} and f_{bD} differ mostly only very slightly for both mixing scenarios (see supplementary material, Table ~~S2~~ S1 and spreadsheet file), which is due to high f_{bD}. For F3, where f_{bD} is near 1, the difference in r_{N2O} does not exceed

Kod pola został zmieniony

0.02, and for F1 with the lowest f_{bD} of ca. 0.7, the difference in r_{N2O} reaches 0.22 (Table ~~S2~~S1). Below we summarize the results of calculations assuming bD-fD mixing scenario only.

The calculation has been performed with two cases (see Section 2.5) and all results are shown and compared with reference method in Table ~~2~~3 and ~~3~~4. Due to quite high f_{bD} for our study the both cases show only very slight differences (Table ~~2~~3, ~~Table3~~Table 4). For the field study F1 we obtained the highest r_{N2O} values (0.86±0.12) and the lowest f_{bD} values (0.74±0.07). For field study F2, the r_{N2O} values were lower (0.38±0.05) and the f_{bD} values were higher (0.92±0.04). For field study F3 the r_{N2O} values were very similar as in F2 (0.33±0.07) and the highest f_{bD} values were noted (0.99±0.01). For the laboratory incubation studies we obtained slightly lower ($p=0.086$) r_{N2O} for L1 (0.19±0.03) when compared to L2 (0.27±0.12). Both laboratory treatments showed very high f_{bD} for L1 (0.99±0.01) and L2 (0.98±0.04).

3.6 SP/N Map

Fig.2

For the SP/N Map we present the literature endmember values in relation to the respective precursor, i.e. NO_3^- for bD and fD and NH_4^+ for nD and Ni (~~supplement,~~ Table S1). For the field and laboratory studies, separate mean values for NO_3^- (11.9 and 4.5 ‰ respectively) and NH_4^+ (41.4 and 79.3 ‰, respectively) were applied. These precursor isotopic signatures are the means of 5 samplings for each campaign and experiment. The extremely ^{15}N enriched $\delta^{15}N_{NH4}$ values result in large shift of endmember ranges for nD and Ni. These ranges are ^{15}N depleted in relation to bD when assuming identical $\delta^{15}N$ values for NO_3^- and NH_4^+, according to most previous studies (Ibraim et al., 2019; Koba et al., 2009; Toyoda et al., 2011). But in the case of our experiments, conversely, N_2O originating from nD and Ni would be significantly enriched in ^{15}N when compared to bD and fD (Fig. 2). For the samples the measured bulk $\delta^{15}N_{N2O}$ is plotted.

The majority of the samples is located outside the area limited by reduction and bD-fD mixing lines, which mostly precludes the application of calculation approach based on SP/N Map. The separation of mixing and reduction processes is not possible based on this plot, since the slopes of reduction line and bD-Ni mixing line are too similar, especially for laboratory experiments (Fig. 2B).

Another approach to include N precursors values is to apply the individual endmembers isotopic signatures for each N_2O sample by interpolating the measured isotopic signatures of NO_3^- and NH_4^+. With 5 measurements of mineral N isotopic signatures per experiment we get quite a good resolution of these values. Since they show quite high variations (Table ~~2~~1) applying individual values is a better approach. But still, also by this approach the majority of samples show values out of the calculation range and the results are very ambiguous representing the whole range of possible variations in both r_{N2O} and f_{bD} values. Therefore these values are not summarized here.

3.7 O/N Map

Fig.3

For O/N Map (Fig.3) the $\delta^{18}O$ values for bD, fD and nD are expressed in relation to soil water and the $\delta^{15}N$ values for bD and fD in relation to soil NO_3^- and for nD and Ni in relation to soil NH_4^+ (~~supplement,~~ Table S1). For these graphs, it is difficult to determine the reduction-mixing area because the slope of the reduction line is almost identical to the bD-fD mixing line.

A significant linear correlations has been found both for the field and laboratory studies, with $R^2=0.27$ ($p<0.1$) and $R^2=0.40$ ($p<0.01$), respectively. Both correlations show similar linear equations: $\delta^{18}O = 0.24* \delta^{15}N +33.3$ and $\delta^{18}O = 0.28* \delta^{15}N +41.6$, for field and laboratory studies, respectively (Fig. 3).

3.8 3DI model

The application of Maps applying $\delta^{15}N$ data, *i.e.*, SP/N and O/N Map, is very imprecise for this case study due to untypically high $\delta^{15}N_{NH4}$ values and shifted location of the nD and Ni mixing endmembers (Fig. 2, Fig. 3) when compared to cases when similar $\delta^{15}N_{NH4}$ and $\delta^{15}N_{NO3}$ values are determined or assumed. However, still the $\delta^{15}N$ data comprise important information, which can assist in processes identification when applied jointly with the SP/O Map. Therefore, we combined all the information in one 3DI model where all three isotopic signatures are taken into account.

The results of this model regarding r_{N2O} are mostly well comparable to the values obtained with SP/O Map (Table ~~2~~3). However, whereas for SP/O Map both Case 1 and Case 2 provide similar results for r_{N2O}, for 3DI model these differ more pronouncedly. On the ~~pie diagrams~~bar plots (Fig. 4) ~~the differences in the calculation assumptions for both cases can be visually compared. In Case 1, the N₂ fraction originates from f_{bD} only, whereas in Case 2 it originates from all the fractions~~we summarize the results obtained from both modeling cases and~~.~~ ~~Bb~~elow we summarize the results of Case 2, which provides more reliable results, as further discussed (see Section 4.2).

We get much more detailed estimation regarding mixing proportions with 3DI model when compared to the SP/O Map. The dominating N_2O production pathway is clearly bD, which contributes in N_2O production from 46 % for F2 up to 69 % for L2 (Fig. 4). An important role plays also nD contributing from 15% for L2 up to 40% N_2O for F3; low f_{nD} of 4% was found for F1. The f_{fD} is quite variable from 6% for F3 to 26% for F1. Ni shows the lowest contribution around 3-5%, and only slightly higher f_{Ni} of 13% was found for F2 (Fig. 4). N_2 fluxes are highly variable between the experiments, *i.e.,* mean r_{N2O} values vary from 0.21 for L1 to 0.89 for F1 (Fig. 4, Table ~~2~~3).

Fig. 4

The model provides very detailed information on probability distribution of the results, which is presented on the matrix plots prepared after Parnell et al. (2013) (~~Fig. 5 shows example plots, all plots are shown in the~~ supplement, Fig. S4), where histograms of probability distribution of r_{N2O} and mixing proportions, correlations between the modeled fractions and R coefficients of these correlations are presented (Fig.~~5~~S4). This summary provides an overview of the reliability of the model outputs and allows for identifying unavoidable model inadequacy. For all the modeled random samples we observe very strong negative correlation between f_{bD} and f_{nD}, similar for both cases, from -0.28 to -0.93, mean -0.63, and between f_{bD} and f_{fD} from -0.15 to -0.97, mean -0.74. r_{N2O} for Case 2 is always correlated negatively with f_{bD} from -0.15 to -0.84, mean -0.62, and positively with f_{fD} from 0.18 to 0.82, mean 0.62. For Case 1 this correlation is extremely variable for r_{N2O}/f_{bD} from -0.67 to 0.85 and for r_{N2O}/f_{fD} from -0.72 to 0.69. The lowest correlation coefficients are noted for f_{Ni}, where mean values never exceed 0.4. This is reflected in the determined ranges of possible results presented in the histograms. f_{Ni} range is typically much narrower than f_{bD} and f_{nD} ranges.

The correlations and histograms vary between the particular campaigns with some typical features. ~~Therefore, in Fig. 5 we present a representative example of the correlation matrix plots for each campaign. The samples with complete repetitive measurements and lowest variations within the repetitions were chosen to present the most representative picture not affected by individual outliers~~. For F1 we observe a very similar output for Case 1 and Case 2, quite narrow ranges of results and no extremely high correlations. For F2 the ranges are much larger and high negative correlations f_{bD} / f_{nD} and f_{fD} / f_{Ni} indicate possible imprecision in separation of these pathways, which results in much wider range of probable results. For F3 the most extreme negative correlation f_{bD} / f_{nD} is noted, and for Case 1 also r and f_{nD} shows very strong correlation, which may affect the proper estimation of r_{N2O}. For L1 and L2 we observe lower correlation f_{bD} / f_{nD} but higher f_{bD} / f_{fD} which is probably a result of different $\delta^{15}N$ endmember values for nD and Ni and better separation of these pathways. The strong positive correlation of r_{N2O} and f_{bD} for Case 1 in L1, F2 and F3 is rather a logical consequence of the assumptions underlying the Case 1 approach.

~~Fig. 5~~

3.9 Comparison of r_{N2O} with independent estimates

The N$_2$O reduction progress calculated with the above presented SP/O Map and 3DI model were compared with the results from the ^{15}N gas-flux method. In the tables below we present the detailed comparison with the results applying both calculation cases (Case 1 and Case 2) for r_{N2O} (Table ~~2~~3) and for mixing proportions (Table ~~3~~4).

Table ~~2~~3

The ranges and the mean values of the replicates means of all sampling dates are quite well comparable for SP/O Map and 3DI model Case 2. Most inconsistent results are obtained in Case 1 of 3DI model, however, for L2 this case seem to be most accurate.

Since the variations of r_{N2O} values in the experiments are very variable in time just a comparison of overall mean values is not informative, we need to compare the temporal changes of r_{N2O} (Fig. 6̶5).

Fig.6̶5

Most extreme changes in time are reported for the laboratory experiment L2 where a very sudden change in r_{N2O} was observed as a consequence of water addition (between sampling 5 and 6). All three estimates present the same trend as the reference method, however, with lower amplitude of the temporal change (Fig. 6̶B̶5B). For field study F3 ^{15}N treatment indicates a constant decrease in r_{N2O}, which is only partially reflected in SP/O Map and not at all in 3DI model results. F1 and F2 data are not complete due to N_2 fluxes under detection limit for the whole F1 sampling and half of the samples of F2 campaign. However, for this missing data we can make estimates of the r_{N2O} based on the known detection limit for N_2 flux. We estimated the r_{N2O} values for the missing points assuming the possible N_2 flux: from 0 up to detection limit of 11.3 gN N_2 ha^{-1} d^{-1}.

Fig.7̶6

In Fig. 7̶6 we checked the fit of r_{N2O} values determined by ^{15}N gas-flux and 3DI model (Fig. 7̶A̶6A) or SP/O Map (Fig. 7̶B̶6B). When analysing all the individual sampling dates or all experiments, the fit to 1:1 line is not very well, especially for many dates of the L2 experiment r_{N2O} is largely underestimated with isotopocule approaches. This is mostly due to the sudden change in r_{N2O} as presented above (Fig. 6̶B̶5B). But when we compare the means of the whole experiment or the experimental phases before and after water addition for L1 and L2 (red points in Fig. 7̶6), the fit is much better with all points within the error of 0.15 for 3DI model. For SP/O Map the L2 mean after irrigation still shows larger disagreement.

The agreement between isotopocule methods and reference method was statistically checked with F value (Eq. 1̶7̶19). The results for all means, minimal and maximal values are shown in Table 2̶3. The statistically significant agreement was ̶p̶r̶o̶v̶e̶d̶ indicated for SP/O Map ($p<0.1$) and Case 2 of 3DI model ($p<0.05$), whereas Case 1 of 3DI model shows no agreement. Particular F values calculated with all sampling dates means indicate no significant agreement (F=0.13 for F3, F=0.45 for L1, F=0.28 for L2 – values for fit between Case 2 of 3DI model and reference method), which reinforces the observation based on Fig.7̶6, that only mean experimental values show good agreement with the reference method, but not the individual samplings.

20

3.10 Comparison of mixing proportions with independent estimates

The mixing proportions obtained by different approaches are much more complex to compare than r_{N2O} due to the fact that each approach provides distinct information.

- With the reference method – ^{15}N gas-flux – we determine the ^{15}N-pool derived fraction of N$_2$O (f_{P_N2O}), hence for the ^{15}NO$_3^-$ treatment this is the fraction of N$_2$O originating from the labeled ^{15}NO$_3^-$ pool. Theoretically, this can be bD or fD. It was intended to use the ^{15}NH$_4^+$ treatment for the determination of N$_2$O fraction derived from NH$_4^+$ pool but due to rapid NH$_4^+$ turnover into NO$_3^-$, we deal with a highly ^{15}N-labeled NO$_3^-$ pool in the ^{15}NH$_4^+$ treatment and hence are not able to precisely separate these pools (results not shown).

- With SP/O Map we determine the f_{bD} fraction. But since in the SP/O Map bD and nD cannot be distinguished due to overlapping isotopic signatures (Fig. 1) this fraction actually informs about bD+nD fraction.

- With the 3DI model we are able to theoretically determine most of the fractions contributing to the N$_2$O flux, but the precision of such determination depends on the isotopic separation of particular pathways in 3D isotopocule plot. In our case study this separation is not very good, especially for δ^{15}N (see Section 3.6 and 3.7), hence this determination is associated with pronounced uncertainty (Fig.~~5~~S4).

To compare all this results we present a comparison f_{P_N2O} of ^{15}N gas-flux (representing bD+fD) with f_{bD} of SP/O Map (representing bD+nD) and respective results ($f_{bD}, f_{bD+fD}, f_{bD+nD}$) of the 3DI model (Fig.~~8~~7, Table ~~3~~4).

Table ~~3~~4

Fig. ~~8~~7

The reasonable agreement in the ranges of values is obtained for experiments L1, L2 and F3, but a large disagreement with the reference ^{15}N gas-flux method is observed for field studies F1 and F2 (Table ~~3~~4). For these studies, extremely low f_{P_N2O} was found by the ^{15}N gas-flux method, of 0.28 and 0.23, respectively. The time dynamics are not very well reflected by various approaches (Fig.~~8~~7). This is mostly visible in F3 (Fig. ~~8~~7E) where the f_{bD} and f_{bD+fD} show large variations between samplings from below 0.1 to above 0.9. These rapid changes show much lower amplitudes according to the ^{15}N gas-flux approach. The contribution of f_{bD+nD} determined by the 3DI model as well as f_{bD} determined by the SP/O Map are much more stable in time, which is especially clear for F3 (Fig. ~~8~~7E), but also true for other campaigns (Fig.~~8~~7).

665 For the mixing proportions the statistical agreement with *F* value (Eq. ~~17~~19) cannot be determined because the fractions provided by various approaches do not precisely refer to the identical pathways contributions and are not directly comparable.

4. Discussion

4.1 Mapping approaches for N$_2$O data interpretation – opportunities and limitations

670 So far the interpretations of N$_2$O isotope data are most commonly done with dual isotope plots. Whereas SP/N and O/N plots were applied in numerous studies before (Kato et al., 2013; Koba et al., 2009; Opdyke et al., 2009; Ostrom et al., 2007; Ostrom et al., 2010; Toyoda et al., 2011; Well et al., 2012; Yamagishi et al., 2007; Zou et al., 2014) the usage of the SP/O plot is quite a new idea (Lewicka-Szczebak et al., 2017), but already used for field studies (Buchen et al., 2018; Ibraim et al., 2019; Verhoeven et al., 2019). The recent work basing on

675 archival datasets with independent estimates of N$_2$ flux showed some weak accordance of the results of the SP/O Map with independent estimates (Wu et al., 2019). However, the reasons are difficult to identify for archival data. Here we present the performance of mapping approaches validated with independent estimates based on ^{15}N gas-flux method and try to identify potential problems.

The first challenge, especially for field studies, is obtaining complete datasets. This is due to limited sensitivity

680 of the isotopic measurements and a need for sufficient N$_2$O and N$_2$ flux. For our first field study (F1), N$_2$ flux was under the detection limit and the r_{N2O} values can thus not be fully compared. For the F2 field study we have numerous missing data due to N$_2$O or N$_2$ flux under detection limit, hence only a limited number of data can be compared. This may be the main reason (besides other discussed later – Section 4.4) for the weakest accordance of the results for F2. For this field study only four samples showed the N$_2$ flux above the detection limit and

685 these measured N$_2$ fluxes associated with the low N$_2$O fluxes yield very low r_{N2O} values. For samples with N$_2$ flux below the detection limit the estimated r_{N2O} ranges show possibly also much higher values (Fig. ~~6D~~5D). Hence, possibly by missing the measurements of low N$_2$ fluxes we miss the higher r_{N2O} values and our calculated means are not representative for the whole experiment (Table ~~2~~3).

690 SP/O Map

The SP/O Map was proposed (Lewicka-Szczebak et al., 2017) after it was found that δ^{18}O of the N$_2$O produced by bacterial and fungal denitrification is quite stable and together with SP may be useable for discrimination of these pathways (Lewicka-Szczebak et al., 2016; Rohe et al., 2014a). As O-precursor for bD, fD and nD the soil water is accepted, under the assumption of nearly complete O-exchange between water and denitrification

695 intermediates. The high extent of O-exchange during denitrification has been confirmed experimentally (Kool et al., 2009; Lewicka-Szczebak et al., 2016; Rohe et al., 2014b) and it results in a quite stable range for mixing

22

endmember values for $\delta^{18}O$ for bacterial and fungal denitrification (Fig. 1). Importantly, due to higher isotope fractionation effect associated with subsequent reduction steps of NO_3^- to N_2O (i.e. removal of oxygen atoms, so called branching effect) during fungal denitrification, the ranges for $\delta^{18}O$ of bacterial and fungal N_2O differ significantly (Lewicka-Szczebak et al., 2016). Fungal denitrification shows very consequent high O-exchange and high fractionation during O-branching (Rohe et al., 2014b; Rohe et al., 2017), whereas bacterial denitrification is characterized in general by lower fractionation, but the differences in both fractionation and O-exchange between particular bacterial strains are large (Rohe et al., 2017). As a result of lower O-exchange showed by some bacterial strains, $\delta^{18}O_{NO3-}$ is also incorporated into produced N_2O (Rohe et al., 2017). This complicates the application of the proposed SP/O Map. It is not clear how large is the importance of such bacterial strains characterized by low O-exchange in soil communities. We assume it must be low, because soil incubation studies indicated so far mostly very high exchange rates (Kool et al., 2007; Kool et al., 2009; Lewicka-Szczebak et al., 2016). These studies covered in total 16 soils and only for two forest soils characterized by very low N_2O emission the O-exchange was around 20 % (Kool et al., 2009), otherwise over 60 %, with mean of around 90 % (Kool et al., 2009; Lewicka-Szczebak et al., 2016). Importantly, the range of $\delta^{18}O$ values determined for bacterial denitrification does not assume complete O-exchange but is determined for the soil samples of O-exchange varying in the range from 63 to 100% (Lewicka-Szczebak et al., 2016). Hence, based on current knowledge, this can be assumed typical for most soils and experimental conditions. Also in this study, quite a good agreement of the r_{N2O} determined by the O/SP Map and the reference method (see Section 3.9) allows us to confirm the general assumption underlying this calculation method.

SP/N Map

The application of dual isotope plot SP/N was initially proposed by Yamagishi et al. (2007) for ocean waters and by Koba et al. (2009) for groundwater studies. In open water bodies, the application of SP/N Map might be effective due to relatively homogenous distribution of substrates in the sampled water volume and thus not biased by the spatial heterogeneity in ^{15}N enrichment that can occur in soils due to the fractionation processes in soil microsites (Bergstermann et al., 2011; Cardenas et al., 2017; Castellano-Hinojosa et al., 2019; Lewicka-Szczebak et al., 2015; Well et al., 2012). The $\delta^{15}N$ isotopic signatures of samples were corrected for NO_3^- substrate only and for water studies this approach was well justified by the complete conversion of NH_4^+ to NO_3^- (Koba et al., 2009). This assumption was based on the low NH_4^+ concentration and should result in equal $\delta^{15}N$ of NH_4^+ and NO_3^-, which allowed to put the whole data into a single $\delta^{15}N^{SP}$ - $\delta^{15}N$ scheme. But for soil studies, due to multiple possible N substrates and difficulties to find a proper correcting strategy, later studies rather applied bulk measured $\delta^{15}N$ without corrections (Kato et al., 2013; Toyoda et al., 2011). Up to now, the most appropriate approach of taking precursors into account is the recalculation of literature mixing endmember values to the actually measured substrate values for each particular pathway, namely NO_3^- for denitrification and

NH$_4^+$ for nitrification (Zou et al., 2014). But this approach was not successful for this study (see Section 3.6). When endmember mixing areas where recalculated with the measured substrate isotope signatures, most of the sampling points were located outside the mixing-reduction area. This is most probably due to large variations in isotopic signatures of the substrates and the fact that the analyzed bulk δ^{15}N values are not representative for the actually utilized substrate pools due to spatial heterogeneity of fractionating processes as outlined above. Moreover, the range of values for NH$_4^+$ and NO$_3^-$ of our studies resulted in a very untypical location of endmember ranges for denitrification and nitrification on the Maps (Fig. 2, Fig. 3), hence the method is not really suitable for discriminating mixing of these pathways and N$_2$O reduction for this particular study. This is due to the extremely high δ^{15}N$_{NH4}$ values (even up to 100‰) which are associated with low NH$_4^+$ contents (Table 12). This indicates that the ammonium pool was highly fractionated and nearly exhausted. This fast ammonium consumption will be further investigated in the follow up paper applying Ntrace model, where we also apply the ^{15}NH$_4$ treatment for its proper interpretation (Müller et al., 2014).

O/N Map

After it was observed that N$_2$O reduction results in the typical O/N slope of 2.6 (Menyailo and Hungate, 2006; Ostrom et al., 2007; Well and Flessa, 2009) the O/N Map was proposed for identification of significant N$_2$O reduction based on the observed slope higher than 1 (Opdyke et al., 2009; Ostrom et al., 2007). However, it must be noted that in case of temporal shifts in the isotopic composition of the N or O substrate the assessment of the importance of N$_2$O reduction is not valid (Ostrom et al., 2010). This approach was well suited for short term controlled experiments, however for longer filed studies, where we deal with large variations of N substrates isotopic signatures, application of this approach appears problematic. We plotted our data in the O/N Map and found a significant linear relationship for field and laboratory studies, both with a very similar equations. The observed slopes of 0.24 and 0.28, respectively, are much below 1, although the N$_2$O reduction shows important contribution for these experiments (Table 23). Hence, this observed slope is rather due to change of active substrate pool or changes in the isotopic fractionation (Cardenas et al., 2017). This might be a result of changes in soil moisture during experiments (irrigation or rain episodes) and between the experiments and field campaigns. The observed shift in δ^{15}N is ca. four times larger than for δ^{18}O. We suppose that water addition intensified N$_2$O production and this might have caused significant enrichment in active nitrate pool in soil microsites. For O isotopes intensified N$_2$O production may result in slightly lower O-exchange, which may increase the δ^{18}O values as a result of incorporation of nitrate O signature (Lewicka-Szczebak et al., 2015; Rohe et al., 2017). Consequently, the isotope effects due to reduction are significantly interfered by shifts in N$_2$O precursors dynamics. Since for this Map both N and O isotopes depend on the precursor isotopic signature and are significantly altered by the diffusion (Well and Flessa, 2008), the interpretations based on this Map are the most ambiguous.

24

4.2 Three-dimensional N$_2$O isotopocule model – perspectives of this new approach

Such a model for interpretation of N$_2$O isotopic data is proposed here for the first time. This model is based on the Bayesian mixing models being well established and widely applied method in food-web studies to partition dietary proportions (Parnell et al., 2013; Phillips et al., 2014). But for N$_2$O the determination of mixing proportion of different pathways contributing to N$_2$O production is further complicated by N$_2$O reduction which alters the final N$_2$O isotopic signature. This additional parameter was incorporated into the model equations (eq. 1013, 1114). Moreover, it is still not clarified, if the reduction of N$_2$O produced during bacterial denitrification only is possible (Case 1) or also N$_2$O from other pathways can be further reduced by bacterial denitrifiers (Case 2), hence both cases need to be considered. The model has a few advantages over the SP/O Map. First of all, it allows for including uncertainties of input data into the model and allows for assessment of the confidence intervals for the results. Moreover, theoretically the 3DI model allows for separation of four N$_2$O production pathways, currently identified as the most relevant, within them f_{fD}, which is so far not distinguishable with other isotopic methods (Wrage-Mönnig et al., 2018).

For our case studies, it has been shown that δ^{15}N values are not useful in dual isotope plots for quantitative estimations (Fig.2, Fig.3, Section 3.6 and 3.7) but are helpful to constrain mixing proportions when incorporated into the 3DI model. Since the model bases on probability distribution, it allows for providing estimates even for imprecise data, e.g. as in our case by difficulties in proper determination of δ^{15}N endmember ranges due to very unstable precursor isotopic signatures.

The model outputs allow us to assess the quality of model performance and reliability of the results (Fig. 5S4, Section 3.8). From the uncertainty analysis provided by the model, we can determine the confidence intervals for the estimated values (Fig. 65, Fig. 87). This is a total uncertainty resulting from all possible uncertainty sources due to: ranges of endmember values and fractionation factors, variations in N$_2$O isotopic signatures for one sampling date, and convergence of possible model results for three isotopic signatures. We are not able to separate these uncertainties in this study.

Another measure of model performance is given by the correlations between obtained results of all the modeled probable solutions (Fig. 5S4). Previous studies applying similar models interpreted the strong negative correlations between determined mixing proportions as inability of the model to distinguish these sources (Moore and Semmens, 2008; Parnell et al., 2013; Phillips et al., 2014). We observe strong negative correlations between f_{bD} and f_{nD} for most cases. This may indicate the uncertainty in determination of these fractions due to the lack of isotopic separation of these processes in the δ^{15}N^{sp}/ δ ^{18}O space (Fig. 1). But such a correlation is also expected if we deal with two strongly dominating sources, and the correlations between f_{bD} and f_{nD} are indeed highest for F3, where the fractions of other pathways are lowest. Nevertheless, for fractions showing high correlations, presentation of the sum of these both pathways may be much more informative than separation

between them. Therefore, we observe much more stable results for the sum of f_{bD} and f_{nD} than for f_{bD} alone (Fig. ~~8~~7). However, the large variations of f_{bD} are not only the modeling artifact, since they reflect the variations noted

800   with the reference method, which is especially clear for F3 (see Fig. ~~8E~~7E). In this case study, we can see that the variations of f_{bD} are larger than in the reference method but similar dynamics of these variations can be observed.

With the model we can quantify the contribution of four pathways, however, there are so far no precise enough reference methods to validate these results (Wrage-Mönnig et al., 2018) (see Section 3.10). But are the provided

805   estimates plausible? We can check with the most characteristic outcomes. For F1 the highest f_{fD} values were noted (Fig. 4~~H~~). For this field study also the highest r_{N2O} and the lowest f_{bD} were noted ~~with~~ by all the ~~methods~~approaches (Table ~~2~~3, Table ~~3~~4, Fig. ~~6C~~5C, Fig. ~~8C~~7C). Since for fD N_2O is mostly the final product not further reduced to N_2 (Sutka et al., 2008), the higher f_{fD} should result in higher r_{N2O} values, which was noted for F1. The highest f_{Ni} was noted for F2. In this field study, the soil ammonium content is clearly the highest and

810   nitrate the lowest (Table ~~1~~2), which indicates that nitrification can be more active here during the whole study campaign, when compared to the other experiments, where we deal with large ammonium consumption at the very beginning of the experiments. This accordance of results allows us to suppose that the general trends in pathways mixing proportions provided by the model is plausible.

4.3 Agreement in estimates of isotopocule approaches and independent estimates

815   In general, the both cases of SP/O Map and Case 2 of 3DI model show very similar results, whereas Case 1 of 3DI model indicates always higher r_{N2O} values, hence underestimates N_2 flux (Table ~~2~~3, Fig. ~~6~~5). For the SP/O Map, the application of different calculation cases has little impact on the final results because both cases show very high and quite stable f_{bD}. The contribution of bD is expressed jointly with nD for the SP/O Map, due to their isotopic overlap (see Section 3.5). As a result, the necessary assumption for the SP/O Map is the possible

820   reduction of N_2O originating from these both fractions bD and nD, also for Case 1. Conversely for 3DI model, these both fractions are separated and for Case 1 only bD fraction can be reduced. The r_{bD} values obtained for Case 1 are very low (eg. 0.2 for F2 and 0.15 for F3) but when recalculated to r_{N2O} (for comparison with other results) they get high (eg. 0.58 for F2 and 0.54 for F3, Table ~~2~~3) due to respective f_{bD} values (see Eq. ~~12~~15). Therefore, the r_{N2O} determined by 3DI model Case 1 is very vulnerable to proper determination of f_{bD}. And this

825   fraction is not very precisely determined, as we know from strong correlation found for f_{bD} / f_{nD} (see Section 4.2). Consequently, the imprecise separation of f_{bD} and f_{nD} is the reason for the biased r_{N2O} values for Case 1 3DI model. This bias is not significant when we deal with very high r_{N2O} fraction, as for F1 (Table ~~2~~3) or for very high and stable bD contribution, as for L2 (Table ~~2~~3, Fig. ~~8B~~7B). For Case 2 the lack of precision in f_{bD} and f_{nD} determination do not largely affect r_{N2O} results, since N_2O originating from all pathways can be reduced in this

830   case (Eq.~~11~~14). Hence, in further discussion for 3DI model results we take into account Case 2 outputs only.

26

This observation may also indicate that not only N_2O from heterotrophic bacterial denitrification can be further reduced to N_2. Although previous studies suggested rather the Case 1 to be more accurate (Verhoeven et al., 2019; Wu et al., 2019), our comparison indicates that Case 1 of the 3DI model underestimates the N_2O reduction in most cases (Table ~~2~~3). This may reinforce a recent discussion on nitrifier denitrification mechanisms assuming that heterotrophic bacterial denitrifiers are relevant in reducing NO_2^- from nitrification (Hink et al., 2017). This would support the assumption that N_2O from nD can be further reduced by bD pathway.

The largest discrepancy in r_{N2O} between isotopocule approaches and reference method is noted for F2 (Table ~~2~~3). In this field campaign we deal with very low N_2O fluxes and the reference method indicates very low r_{N2O} values, i.e., very high N_2O reduction rate. Moreover, for F2 the highest soil moisture of the field studies was noted (Table ~~1~~2), which may result in inhibition of gaseous exchange. In these conditions, it is very probable that some of the produced N_2O is completely reduced, and consequently, the isotopic information on its reduction is missed. Complete N_2O reduction in soil microsites would result in overestimation of r_{N2O} values by the N_2O isotopocule approaches and this is what we observe in this case (Fig. ~~6D~~5D).

Pronounced discrepancies in mean values are also noted for L2 laboratory incubation (Table ~~2~~3), which is due to rapid changes in r_{N2O} resulting from water addition (Fig. ~~6B~~5B, Section 4.1). This rapid change is noted in both SP/O Map and 3DI model and in the reference method, but the N_2O isotopocule results seem to react slower and with lower amplitude. N_2O isotopocule approaches base on isotopic analyses of N_2O, whereas ^{15}N gas-flux method base on the direct N_2 measurements. If N_2O is partially stored in soil we may deal with delay in our observations or discrepancy in results. This indicates that individual sudden changes are not well monitored by the isotopocule approaches but the general mean values and changing trends are very well reflected (Table ~~2~~3, Fig. ~~7~~6).

Summary statistics for agreement between isotopocule approaches and reference method indicate significant fit for SP/O Map, where both cases show very similar fit, and for 3DI model Case 2, where the best fit was observed (Table ~~2~~3). This agreement is much better than recently shown by Wu et al. (2019), where numerous cases with very poor agreement between the results of O/SP Map and reference method have been found. That study analyzed archival datasets, from which many experiments consisted of various experimental phases – like anoxic and oxic or before and after fertilizer addition. This might have complicated the comparability of the results. As shown by our study, the sudden changes in experimental conditions are differently reflected in the results of both methods. Whereas the reference method based on direct measurements of N_2 flux reacts immediately, results of isotopocule approaches show a certain delay, possibly due to accumulation of N_2O in the soil (Fig. ~~6B~~5B). But when we compare the mean values for each experimental phase, the agreement between both methods is much better (Fig. ~~7~~6). Additionally, the former study included some experiments with glucose amendment (Wu et al., 2019), which results in a very rapid N turnover and in consequence unstable pathways contribution.

865 The source partitioning of N$_2$O production seems much more problematic than of r_{N2O} values. This is also more difficult to be evaluated with the reference method since it yields only the sum of fD and bD, *i.e.*, it does not distinguish these individual processes (see Section 3.10). We are also aware that the model may not be very precise in separation of f_{bD}, f_{nD} and f_{fD}, since they often show strong negative correlation (see Section 3.8 and 4.2). Taking these considerations into account, we can well understand the fractions contribution for L1, L2 and

870 F3, where the f_{bD} fraction of SP/O Map and f_{bD+nD} of 3DI model are comparable and f_{bD+fD} of the 3DI model and f_{P_N2O} of the ^{15}N gas-flux method show similar range and trends (Fig. ~~8A~~7A, ~~8B~~7B, ~~8E~~7E). However, a large bias in source partition is observed for F1 and F2 field studies. The f_{P_N2O} determined by ^{15}N gas-flux method is much lower than any fraction determined with isotopocule methods (Fig. ~~8C~~7C, ~~8D~~7D). The very low f_{P_N2O} fraction indicates large contribution of N$_2$O originating from unlabelled pool, since the f_{P_N2O} of the labeled

875 ^{15}NH$_4^+$ treatment was also comparably low (data not shown). This N$_2$O may originate from organic N pool pathway (Müller et al., 2014; Zhang et al., 2015) or chemodenitfication (Wei et al., 2019). These processes are not included in the isotopocule methods hence cannot be accounted for. For these two field studies F1 and F2 we deal with relatively low fluxes and low temperatures, thus the processes invisible for high flux situations may play significant role here.

880 **4.4 Possible origins of inconsistency and potential improvements**

From the comparison of isotopocule approaches and the reference method we can identify the condition when the calculation based on natural abundance N$_2$O isotopes may be biased. The Maps applying δ^{15}N value are very vulnerable to changes in substrate isotopic signatures. When we observe large variations in soil NO$_3^-$, NO$_2^-$ or NH$_4^+$ isotopic signatures such approach should rather not be applied.

885 Most problematic is the occurrence of N$_2$O production pathways which are so far not investigated for their characteristic isotopic signature. This might be heterotrophic nitrification, co-denitrification or chemodenitrification, as supposed for our case studies F1 and F2. These less examined processes gain on significance when the N$_2$O fluxes are generally low, like in F1 and F2, where N$_2$O flux was mostly below 10 gN-N$_2$O ha^{-1}d^{-1}. Hence, for such low N$_2$O fluxes application of isotope Maps and 3DI model ~~is~~ may be less precise.

890 Recent literature suggest that the most vulnerable value for SP/O Map is the isotopic signature of the bD mixing endmember and this parameter should be best determined in focused experiments (Buchen et al., 2018; Wu et al., 2019). It was shown that a short-term anoxic experiment with N$_2$O reduction inhibition with C$_2$H$_2$ favors bD (Lewicka-Szczebak et al., 2017; Lewicka-Szczebak et al., 2016). Such an experiment could have been used for determination of isotopic signature of bacterial denitrification characteristic for the particular soil used in this

895 study and narrow the range of mixing endmember for bD pathway. Unfortunately, when planning and conducting these studies we did not have this complete knowledge and missed to perform such parallel anoxic incubations, but this should be strongly recommended for further studies applying SP/O Map or 3DI model.

The determination of initial delta values (δ_0), unchanged by N_2O reduction might be also helpful in further constraining the isotope Maps. These δ_0 can be obtained from the relation of r_{N2O} determined by reference method and measured isotopic signatures (Lewicka-Szczebak et al., 2017). Unfortunately, this approach was not successful for our data, because no significant correlation between r_{N2O} and isotopic signatures could be found. This indicates unstable endmembers mixing proportions or some problems with parallel experiments. This was also the case in previous validation experimental study (Lewicka-Szczebak et al., 2017), where for oxic conditions the variations were too high to obtain significant correlation and determine the δ_0 values. This shows that oxic experiments are not well suited for determination of isotopic signatures of particular mixing endmembers and should be always accompanied by more focused and stable anoxic incubations.

Further enhancement in performance of the isotope Maps could be attained if the experiments determining the initial isotopic composition of mixing endmembers were performed with the soil collected parallel to particular experiments and the anoxic incubations were performed in the conditions similar to field conditions during the particular case study. Possibly from such experiments some subtle differences in characteristic endmember isotopic signatures would be detected. It can be supposed that such differences could be the reason for worse r_{N2O} agreement with reference method for L2 and F2 (Table 2~~3~~). It has been shown that the changes in initial $\delta^{18}O$ value of bacterial denitrification endmember has significant impact on the final results (Wu et al., 2019). We have checked if this could bring better agreement . For L2 the perfect agreement of SP/O Map and reference method is obtained when applying slightly higher $\delta^{18}O$ values: 25 ‰ instead of 19~~.3~~ ‰. Conversely for F2, much lower $\delta^{18}O$ values: 10 ‰ instead of 19 ~~.3~~‰ would be needed to obtain the perfect agreement. This differences are quite possible, the low values for F2 might be a result of low temperature and low fluxes, and in consequence moderate or slow processes associated with maximal O-exchange. On the contrary, for high water content and high temperature in L2 experiment we can expect slightly lower O-exchange resulting in higher initial $\delta^{18}O$ values.

Conclusions

- It was shown that N_2O residual fraction can be calculated based on isotope fractionation during N_2O reduction with SP/$\delta^{18}O$ Map~~ping approach~~. The SP/$\delta^{15}N$ Map~~ping approach~~ appeared more complex and problematic.

- Here we present for the first time the idea of applying ~~triple isotope plot and develop~~ a model based on ~~all~~ three N_2O isotopic signatures. We are convinced that this is a powerful step forward in development of N_2O isotopocule methods to quantify especially r_{N2O}, but also estimate some mixing proportions of the four N_2O pathways included in the model.

- Both N_2O isotopocule based approaches - SP/O Map and 3DI model (Case 2) – show good accordance of r_{N2O} with reference method and very comparable results to each other. For 3DI model the results ~~of Case 2 (assuming possible N_2O reduction of all N_2O production pathways) were taken into account, since the results~~ of Case 1 (assuming N_2O reduction of bacterial denitrification only) underestimate the N_2 flux due to imprecision in determination of f_{bD}.

- The determination of mixing proportions with N_2O isotopocule based approaches is biased for cases where additional processes not incorporated into the model occur. This may be the case when very low N_2O fluxes are noted.

- N_2 flux determined from ^{15}N labelled treatments (reference method) show more rapid changes compared to values determined with N_2O isotopocule approaches. Hence, the r_{N2O} determined with N_2O isotopocule approaches provides a good approximation of the averaged N_2O reduction range, but do not reflect dynamic changes of r_{N2O} with high resolution.

- ~~For the~~ 3DI model allows~~, the correlation matrix plots allow~~ for a good control of the results quality, which is a clear advantage over the results provided with SP/O Map.

- According to these findings, the SP/O Map and 3DI model can be applied for r_{N2O} determination with expected precision of around 0.1~~5~~. For cases where the mixing proportions separation is imprecise, which can be supposed when model results show high negative correlations, the results should be carefully interpreted and preferably the values of correlated fractions should be shown jointly. In such cases, the calculation Case 2 should be applied for r_{N2O} determination, since Case 1 incorporates possibly biased f_{bD} into the final r_{N2O} value. Importantly, even for these cases where the determination of mixing proportions was biased, we got reasonable estimates of r_{N2O} values (with Case 2 calculations).

References:

970 ~~unpublished data from 15N tracer studies by U. Wolf et al. and L. Rohe et al.~~

Aulakh, M. S., Doran, J. W., and Mosier, A. R.: Field-Evaluation of 4 Methods for Measuring
Denitrification, Soil Sci Soc Am J, 55, 1332-1338, 1991.

Baily, A., Watson, C. J., Laughlin, R., Matthews, D., McGeough, K., and Jordan, P.: Use of the ^{15}N gas
flux method to measure the source and level of N_2O and N_2 emissions from grazed grassland, Nutr
975 Cycl Agroecosys, 94, 287-298, 2012.

Barford, C. C., Montoya, J. P., Altabet, M. A., and Mitchell, R.: Steady-state nitrogen isotope effects of
N_2 and N_2O production in Paracoccus denitrificans, Appl Environ Microb, 65, 989-994, 1999.

Baumgärtel, B. and Benke, M.: Düngeempfehlungen Stickstoff: Getreide, Raps, Hackfrüchte.,
Landwirtschaftskammer Niedersachsen - Geschäftsbereich Landwirtschaft, 2009. 2009.

980 Bergsma, T. T., Ostrom, N. E., Emmons, M., and Robertson, G. P.: Measuring simultaneous fluxes
from soil of N_2O and N_2 in the field using the ^{15}N-Gas "nonequilihrium" technique, Environ Sci
Technol, 35, 4307-4312, 2001.

Bergstermann, A., Cardenas, L., Bol, R., Gilliam, L., Goulding, K., Meijide, A., Scholefield, D., Vallejo,
A., and Well, R.: Effect of antecedent soil moisture conditions on emissions and isotopologue
985 distribution of N2O during denitrification, Soil Biol Biochem, 43, 240-250, 2011.

Böhlke, J. K., Smith, R. L., and Hannon, J. E.: Isotopic analysis of N and O in nitrite and nitrate by
sequential selective bacterial reduction to N_2O, Anal Chem, 79, 5888-5895, 2007.

Bouwman, A. F., Beusen, A. H. W., Griffioen, J., Van Groenigen, J. W., Hefting, M. M., Oenema, O.,
Van Puijenbroek, P. J. T. M., Seitzinger, S., Slomp, C. P., and Stehfest, E.: Global trends and
990 uncertainties in terrestrial denitrification and N_2O emissions, Philos T R Soc B, 368, 2013.

Brenninkmeijer, C. A. M. and Röckmann, T.: Mass spectrometry of the intramolecular nitrogen
isotope distribution of environmental nitrous oxide using fragment-ion analysis, Rapid Commun Mass
Sp, 13, 2028-2033, 1999.

Buchen, C., Lewicka-Szczebak, D., Fuß, R., Helfrich, M., Flessa, H., and Well, R.: Fluxes of N_2 and N_2O
995 and contributing processes in summer after grassland renewal and grassland conversion to maize
cropping on a Plaggic Anthrosol and a Histic Gleysol, Soil Biol Biochem, 101, 6-19, 2016.

Buchen, C., Lewicka-Szczebak, D., Flessa, H., and Well, R.: Estimating N_2O processes during grassland
renewal and grassland conversion to maize cropping using N_2O isotopocules, Rapid Commun Mass
Sp, 32 (13), 1053-1067, 2018.

1000 Butterbach-Bahl, K., Baggs, E. M., Dannenmann, M., Kiese, R., and Zechmeister-Boltenstern, S.:
Nitrous oxide emissions from soils: how well do we understand the processes and their controls?,
Philos T R Soc B, 368, 2013.

Cardenas, L., Bol, R., D., L.-S., Gregory, A. S., Matthews, G. P., Whalley, W. R., Misselbrook, R., Scholefield, D., and Well, R.: Effect of soil saturation on denitrification in a grassland soil, Biogeosciences, 14, 4691-4710, 2017.

Casciotti, K. L., Sigman, D. M., Hastings, M. G., Bohlke, J. K., and Hilkert, A.: Measurement of the oxygen isotopic composition of nitrate in seawater and freshwater using the denitrifier method, Anal Chem, 74, 4905-4912, 2002.

Castellano-Hinojosa, A., Loick, N., Dixon, E., Matthews, G. P., Lewicka-Szczebak, D., Well, R., Bol, R., Charteris, A., and Cardenas, L.: Improved isotopic model based on ^{15}N tracing and Rayleigh-type isotope fractionation for simulating differential sources of N_2O emissions in a clay grassland soil, Rapid Communication in Mass Spectrometry, 33, 449-460, 2019.

Decock, C. and Six, J.: An assessment of N-cycling and sources of N_2O during a simulated rain event using natural abundance ^{15}N, Agr Ecosyst Environ, 165, 141-150, 2013.

Eschenbach, W., Lewicka-Szczebak, D., Stange, C. F., Dyckmans, J., and Well, R.: Measuring [15]N Abundance and Concentration of Aqueous Nitrate, Nitrite, and Ammonium by Membrane Inlet Quadrupole Mass Spectrometry, Anal Chem, 89, 6076-6081, 2017.

Felix, J. D., Elliott, E. M., Gish, T. J., McConnell, L. L., and Shaw, S. L.: Characterizing the isotopic composition of atmospheric ammonia emission sources using passive samplers and a combined oxidation-bacterial denitrifier approach, Rapid Communication in Mass Spectrometry, 27, 2239–2246, 2013.

Firestone, M. K. and Davidson, E. A.: Microbial basis of NO and N_2O production and consumption in soil. In: Exchange of trace gases between terrestial ecosystems and the atmosphere., Andreae, M. O. and Schimel, D. S. (Eds.), John Wiley and Sons, New York, 1989.

Frame, C. H. and Casciotti, K. L.: Biogeochemical controls and isotopic signatures of nitrous oxide production by a marine ammonia-oxidizing bacterium, Biogeosciences, 7, 2695-2709, 2010.

Fuß, R., last access: 10.01.2020, 2015.

Groffman, P. M.: Terrestial denitrification: challenges and opportunities, Ecological Processes, 2012, 1-11, 2012.

Groffman, P. M., Altabet, M. A., Bohlke, J. K., Butterbach-Bahl, K., David, M. B., Firestone, M. K., Giblin, A. E., Kana, T. M., Nielsen, L. P., and Voytek, M. A.: Methods for measuring denitrification: Diverse approaches to a difficult problem, Ecol Appl, 16, 2091-2122, 2006.

Hink, L., Lycus, P., Gubry-Rangin, C., Frostegård, A., Nicol, G. W., Prosser, J. I., and Bakken, L. R.: Kinetics of NH_3 oxidation, NO^- turnover, N_2O^- production and electron flow during oxygen depletion in model bacterial and archaeal ammonia oxidisers, Environ Microbiol, 19, 4882-4896, 2017.

Ibraim, E., Wolf, B., Harris, E., Gasche, R., Wei, J., Longfei, Y., Kiese, R., Eggleston, S., Butterbach-Bahl, K., Zeeman, M., Tuzson, B., Emmenegger, L., Six, J., Henne, S., and Mohn, J.: Attribution of N2O sources in a grassland soil with laser spectroscopy based isotopocule analysis, Biogeosciences, 16, 3247–3266, 2019.

IPCC: Climate Change 2007: The Physical Science Basis. Contribution of Working Group I to the Fourth Assessment Report of the Intergovernmental Panel on Climate Change, 2007.

Jinuntuya-Nortman, M., Sutka, R. L., Ostrom, P. H., Gandhi, H., and Ostrom, N. E.: Isotopologue fractionation during microbial reduction of N_2O within soil mesocosms as a function of water-filled pore space, Soil Biol Biochem, 40, 2273-2280, 2008.

1045   Kato, T., Toyoda, S., Yoshida, N., Tang, Y. H., and Wada, E.: Isotopomer and isotopologue signatures of N_2O produced in alpine ecosystems on the Qinghai-Tibetan Plateau, Rapid Commun Mass Sp, 27, 1517-1526, 2013.

Knowles, R.: Denitrification, Microbiol Rev, 46, 43-70, 1982.

Koba, K., Osaka, K., Tobari, Y., Toyoda, S., Ohte, N., Katsuyama, M., Suzuki, N., Itoh, M., Yamagishi, H.,
1050   Kawasaki, M., Kim, S. J., Yoshida, N., and Nakajimag, T.: Biogeochemistry of nitrous oxide in groundwater in a forested ecosystem elucidated by nitrous oxide isotopomer measurements, Geochimica at Cosmochimica Acta, 73, 3115-3133, 2009.

Kool, D. M., Wrage, N., Oenema, O., Dolfing, J., and Van Groenigen, J. W.: Oxygen exchange between (de) nitrification intermediates and H_2O and its implications for source determination of NO_3^- and
1055 N_2O: a review, Rapid Commun Mass Sp, 21, 3569-3578, 2007.

Kool, D. M., Wrage, N., Oenema, O., Harris, D., and Van Groenigen, J. W.: The ^{18}O signature of biogenic nitrous oxide is determined by O exchange with water, Rapid Commun Mass Sp, 23, 104-108, 2009.

Kramps-Alpmann, D., Ruoss, N., Korte K., Ernst, U., and Schäfer, B. C.: Klimaoptimierte
1060   Anpassungsstrategien in der Landwirtschaft (optimierter Klimabetrieb) II., Unpublished project report, 2017. 2017.

Kulkarni, M. V., Burgin, A. J., Groffman, P. M., and Yavitt, J. B.: Direct flux and ^{15}N tracer methods for measuring denitrification in forest soils, Biogeochemistry, 117, 359-373, 2013.

Lewicka-Szczebak, D., Augustin, J., Giesemann, A., and Well, R.: Quantifying N_2O reduction to N_2
1065   based on N_2O isotopocules - validation with independent methods (helium incubation and ^{15}N gas flux method). , Biogeosciences, 14, 711-732, 2017.

Lewicka-Szczebak, D., Dyckmanns, J., Kaiser, J., Marca, A., Augustin, J., and Well, R.: Oxygen isotope fractionation during N_2O production by soil denitrification, Biogeosciences, 13, 1129-1144, 2016.

Lewicka-Szczebak, D. and Well, R.: The ^{15}N gas-flux method to determine N_2 flux : a comparison of
1070   different tracer addition approaches, SOIL, 6, 145-152, 2020.

Lewicka-Szczebak, D., Well, R., Bol, R., Gregory, A., Matthews, P., Misselbrook, T., Whalley, R., and Cardenas, L.: Isotope fractionation factors controlling isotopocule signatures of soil-emitted N_2O produced by denitrification processes of various rates, Rapid Commun Mass Sp, 29, 269–282, 2015.

Lewicka-Szczebak, D., Well, R., Giesemann, A., Rohe, L., and Wolf, U.: An enhanced technique for
1075   automated determination of ^{15}N signatures of N_2, (N_2+N_2O) and N_2O in gas samples, Rapid Commun Mass Sp, 27, 1548-1558, 2013.

Lewicka-Szczebak, D., Well, R., Koster, J. R., Fuss, R., Senbayram, M., Dittert, K., and Flessa, H.: Experimental determinations of isotopic fractionation factors associated with N_2O production and reduction during denitrification in soils, Geochim Cosmochim Ac, 134, 55-73, 2014.

1080   Maeda, K., Spor, A., Edel-Hermann, V., Heraud, C., Breuil, M. C., Bizouard, F., Toyoda, S., Yoshida, N., Steinberg, C., and Philippot, L.: N_2O production, a widespread trait in fungi, Sci Rep-Uk, 5, 9697: 9691-9697, 2015.

Mandernack, K. W., Mills, C. T., Johnson, C. A., Rahn, T., and Kinney, C.: The $\delta^{15}N$ and $\delta^{18}O$ values of N_2O produced during the co-oxidation of ammonia by methanotrophic bacteria, Chem Geol, 267, 96-
1085   107, 2009.

Mathieu, O., Leveque, J., Henault, C., Milloux, M. J., Bizouard, F., and Andreux, F.: Emissions and spatial variability of N_2O, N_2 and nitrous oxide mole fraction at the field scale, revealed with ^{15}N isotopic techniques, Soil Biol Biochem, 38, 941-951, 2006.

Menyailo, O. V. and Hungate, B. A.: Stable isotope discrimination during soil denitrification: Production and consumption of nitrous oxide, Global Biogeochem Cy, 20, GB3025, 2006.

Moore, J. W. and Semmens, B. X.: Incorporating uncertainty and prior information into stable isotope mixing models, Ecology Letters, 11, 470-480, 2008.

Morse, J. L. and Bernhardt, E. S.: Using ^{15}N tracers to estimate N_2O and N_2 emissions from nitrification and denitrification in coastal plain wetlands under contrasting land-uses, Soil Biol Biochem, 57, 635-643, 2013.

Mosier, A. R., Guenzi, W. D., and Schweizer, E. E.: Field Denitrification Estimation by N-15 and Acetylene Inhibition Techniques, Soil Sci Soc Am J, 50, 831-833, 1986.

Müller, C., Laughlin, R. J., Spott, O., and Rütting, T.: Quantification of N_2O emission pathways via a ^{15}N tracing model, Soil Biol Biochem, 72, 44-54, 2014.

Nash, J. E. and Sutcliffe, J. V.: River flow forecasting through conceptual models part I— a discussion of principles. , J Hydrol, 10, 282-290, 1970.

Opdyke, M. R., Ostrom, N. E., and Ostrom, P. H.: Evidence for the predominance of denitrification as a source of N_2O in temperate agricultural soils based on isotopologue measurements, Global Biogeochem Cy, 23, GB4018: 4011-4010, 2009.

Ostrom, N. E., Pitt, A., Sutka, R., Ostrom, P. H., Grandy, A. S., Huizinga, K. M., and Robertson, G. P.: Isotopologue effects during N_2O reduction in soils and in pure cultures of denitrifiers, J Geophys Res-Biogeo, 112, G02005: 02001-02012, 2007.

Ostrom, N. E., Sutka, R., Ostrom, P. H., Grandy, A. S., Huizinga, K. M., Gandhi, H., von Fischer, J. C., and Robertson, G. P.: Isotopologue data reveal bacterial denitrification as the primary source of N2O during a high flux event following cultivation of a native temperate grassland, Soil Biol Biochem, 42, 499-506, 2010.

Park, S., Perez, T., Boering, K. A., Trumbore, S. E., Gil, J., Marquina, S., and Tyler, S. C.: Can N_2O stable isotopes and isotopomers be useful tools to characterize sources and microbial pathways of N_2O production and consumption in tropical soils?, Global Biogeochem Cy, 25, GB1001, 2011.

Parnell, A. C., Phillips, D. L., Bearhop, S., Semmens, B. X., Ward, E. J., Moore, J. W., Jackson, A. L., Grey, J., Kelly, D. J., and Inger, R.: Bayesian stable isotope mixing models, Environmetrics, 24, 387-399, 2013.

Phillips, D. L., Inger, R., Bearhop, S., Jackson, A. L., Moore, J. W., Parnell, A. C., Semmens, B. X., and Ward, E. J.: Best practices for use of stable isotope mixing models in food-web studies, Canadian Journal of Zoology 92, 823–835, 2014.

Ravishankara, A. R., Daniel, J. S., and Portmann, R. W.: Nitrous Oxide (N_2O): The Dominant Ozone-Depleting Substance Emitted in the 21st Century, Science, 326, 123-125, 2009.

Röckmann, T., Kaiser, J., Brenninkmeijer, C. A. M., and Brand, W. A.: Gas chromatography/isotope-ratio mass spectrometry method for high-precision position-dependent ^{15}N and [18]O measurements of atmospheric nitrous oxide, Rapid Commun Mass Sp, 17, 1897-1908, 2003.

Rohe, L., Anderson, T.-H., Braker, G., Flessa, H., Giesemann, A., Lewicka-Szczebak, D., Wrage-Mönnig, N., and Well, R.: Dual isotope and isotopomer signatures of nitrous oxide from fungal denitrification – a pure culture study, Rapid Commun Mass Sp, 28, 1893-1903, 2014a.

34

Rohe, L., Anderson, T. H., Braker, G., Flessa, H., Giesemann, A., Wrage-Monnig, N., and Well, R.:
1130 Fungal oxygen exchange between denitrification intermediates and water, Rapid Commun Mass Sp, 28, 377-384, 2014b.

Rohe, L., Well, R., and Lewicka-Szczebak, D.: Use of oxygen isotopes to differentiate between nitrous oxide produced by fungi or bacteria during denitrification, Rapid Communication in Mass Spectrometry, 31, 1297-1312, 2017.

1135 Saggar, S., Jha, N., Deslippe, J., Bolan, S., Luo, J., Giltrap, D. L., Kim, D.-G., Zaman, M., and Tillman, R. W.: Denitrification and $N_2O:N_2$ production in temperate grasslands: Processes, measurements, modelling and mitigating negative impacts, Science of the Total Environment, 465, 173-195, 2013.

Schmidt, G., Segschneider H.-J., and R., R.: Bestimmung der 15N Häufigkeit bei nichtstatistischer 15N-verteilung in N2 sowie bei N2O in Bodenluftproben mittels GC-R-IRMS-Kopplung in einem
1140 Probenlauf, Isot Environ Healt S, 34, 235-243, 1998.

Scholefield, D., Hawkins, J. M. B., and Jackson, S. M.: Development of a helium atmosphere soil incubation technique for direct measurement of nitrous oxide and dinitrogen fluxes during denitrification, Soil Biol Biochem, 29, 1345-1352, 1997.

Seitzinger, S.: Nitrogen cycle - Out of reach, Nature, 452, 162-163, 2008.

1145 Senbayram, M., Chen, R., Budai, A., Bakken, L., and Dittert, K.: N_2O emission and the $N_2O/(N_2O + N_2)$ product ratio of denitrification as controlled by available carbon substrates and nitrate concentrations, Agr Ecosyst Environ, 147, 4-12, 2012.

Sigman, D. M., Casciotti, K. L., Andreani, M., Barford, C., Galanter, M., and Bohlke, J. K.: A bacterial method for the nitrogen isotopic analysis of nitrate in seawater and freshwater, Anal Chem, 73,
1150 4145-4153, 2001.

Spott, O., Russow, R., Apelt, B., and Stange, C. F.: A N-15-aided artificial atmosphere gas flow technique for online determination of soil N_2 release using the zeolite Kostrolith SX6 (R), Rapid Commun Mass Sp, 20, 3267-3274, 2006.

Stange, C. F., Spott, O., Apelt, B., and Russow, R. W. B.: Automated and rapid online determination of
1155 ^{15}N abundance and concentration of ammonium, nitrite, or nitrate in aqueous samples by the SPINMAS technique, Isot Environ Healt S, 43, 227-236, 2007.

Stevens, R. J. and Laughlin, R. J.: Nitrite Transformations during Soil Extraction with Potassium-Chloride, Soil Sci Soc Am J, 59, 933-938, 1995.

Sutka, R. L., Adams, G. C., Ostrom, N. E., and Ostrom, P. H.: Isotopologue fractionation during N_2O
1160 production by fungal denitrification, Rapid Commun Mass Sp, 22, 3989-3996, 2008.

Sutka, R. L., Ostrom, N. E., Ostrom, P. H., Breznak, J. A., Gandhi, H., Pitt, A. J., and Li, F.: Distinguishing nitrous oxide production from nitrification and denitrification on the basis of isotopomer abundances, Appl Environ Microb, 72, 638-644, 2006.

Toyoda, S., Mutobe, H., Yamagishi, H., Yoshida, N., and Tanji, Y.: Fractionation of N_2O isotopomers
1165 during production by denitrifier, Soil Biol Biochem, 37, 1535-1545, 2005.

Toyoda, S., Yano, M., Nishimura, S., Akiyama, H., Hayakawa, A., Koba, K., Sudo, S., Yagi, K., Makabe, A., Tobari, Y., Ogawa, N. O., Ohkouchi, N., Yamada, K., and Yoshida, N.: Characterization and production and consumption processes of N_2O emitted from temperate agricultural soils determined via isotopomer ratio analysis, Global Biogeochem Cy, 25, GB2008, 2011.

1170 Toyoda, S. and Yoshida, N.: Determination of nitrogen isotopomers of nitrous oxide on a modified isotope ratio mass spectrometer, Anal Chem, 71, 4711-4718, 1999.

Toyoda, S., Yoshida, N., and Koba, K.: Isotopocule analysis of biologically produced nitrous oxide in various environments, Mass Spectrometry Reviews, doi: 10.1002/mas.21459, 2017. 2017.

Verhoeven, E., Barthel, M., Yu, L., Celi, L., Said-Pullicino, D., Sleutel, S., Lewicka-Szczebak, D., Six, J., and Decock, C.: Early season N2O emissions under variable water management in rice systems: source-partitioning emissions using isotope ratios along a depth profile, Biogeosciences, 16 (2), 383-408, 2019.

Wei, J., Ibraim, E., Brüggemann, N., Vereecken, H., and Mohn, J.: First real-time isotopic characterisation of N_2O from chemodenitrification, Geochim Cosmochim Ac, 267, 17-32, 2019.

Well, R., Burkart, S., Giesemann, A., Grosz, B., Köster, J. R., and Lewicka-Szczebak, D.: Improvement of the ^{15}N gas flux method for in situ measurement of soil denitrification and its product stoichiometry, Rapid Commun Mass Sp, 33, 437-448, 2019a.

Well, R., Eschenbach, W., Flessa, H., von der Heide, C., and Weymann, D.: Are dual isotope and isotopomer ratios of N_2O useful indicators for N_2O turnover during denitrification in nitrate-contaminated aquifers?, Geochim Cosmochim Ac, 90, 265-282, 2012.

Well, R. and Flessa, H.: Isotope fractionation factors of N_2O diffusion, Rapid Commun Mass Sp, 22, 2621-2628, 2008.

Well, R. and Flessa, H.: Isotopologue enrichment factors of N_2O reduction in soils, Rapid Commun Mass Sp, 23, 2996-3002, 2009.

Well, R., Maier, M., Lewicka-Szczebak, D., Köster, J. R., and Ruoss, N.: Underestimation of denitrification rates from field application of the ^{15}N gas flux method and its correction by gas diffusion modelling, Biogeosciences, 16, 2233–2246, 2019b.

Westley, M. B., Popp, B. N., and Rust, T. M.: The calibration of the intramolecular nitrogen isotope distribution in nitrous oxide measured by isotope ratio mass spectrometry, Rapid Commun Mass Sp, 21, 391-405, 2007.

Wolf, B., Merbold, L., Decock, C., Tuzson, B., Harris, E., Six, J., Emmenegger, L., and Mohn, J.: First on-line isotopic characterization of N2O above intensively managed grassland, Biogeosciences, 12, 2517-2531, 2015.

Wrage-Mönnig, N., Horn, M. A., Well, R., Müller, C., Velthof, G., and Oenema, O.: The role of nitrifier denitrification in the production of nitrous oxide revisited, Soil Biology and Biochemistry, 123, A3-A16, 2018.

Wu, D., Well, R., Cárdenas, L. M., Fuß, R., Lewicka-Szczebak, D., Köster, J. R., Brüggemann, N., and Bol, R.: Quantifying N_2O reduction to N_2 during denitrification in soils via isotopic mapping approach: Model evaluation and uncertainty analysis, Environmental Research, 2019. 108806, 2019.

Wu, H. H., Dannenmann, M., Fanselow, N., Wolf, B., Yao, Z. S., Wu, X., Bruggemann, N., Zheng, X. H., Han, X. G., Dittert, K., and Butterbach-Bahl, K.: Feedback of grazing on gross rates of N mineralization and inorganic N partitioning in steppe soils of Inner Mongolia, Plant Soil, 340, 127-139, 2011.

Yamagishi, H., Westley, M. B., Popp, B. N., Toyoda, S., Yoshida, N., Watanabe, S., Koba, K., and Yamanaka, Y.: Role of nitrification and denitrification on the nitrous oxide cycle in the eastern tropical North Pacific and Gulf of California, J Geophys Res-Biogeo, 112, 2007.

Yoshida, N.: ^{15}N-depleted N_2O as a product of nitrification., Nature, 335, 528-529, 1988.

Yu, L., Harris, E., Lewicka-Szczebak, D., Barthel, M., Blomberg, M. R. A., Harris, S., Johnson, M. S., Lehmann, M. F., Liisberg, J., Müller, C., Ostrom, N., Six, J., Toyoda, S., Yoshida, N., and Mohn, J.: What

can we learn from N_2O isotope data? - Analytics, processes and modelling, Rapid Communication in
1215   Mass Spectrometry, 34, e8858, 2020.

Zhang, J. B., Muller, C., and Cai, Z. C.: Heterotrophic nitrification of organic N and its contribution to
nitrous oxide emissions in soils, Soil Biol Biochem, 84, 199-209, 2015.

Zhang, L., Altabet, M. A., Wu, T. X., and Hadas, O.: Sensitive measurement of NH_4^+ $^{15}N/^{14}N$ ($\delta^{15}NH_4^+$)
at natural abundance levels in fresh and saltwaters, Anal Chem, 79, 5297-5303, 2007.
1220   Zou, Y., Hirono, Y., Yanai, Y., Hattori, S., Toyoda, S., and Yoshida, N.: Isotopomer analysis of nitrous
oxide accumulated in soil cultivated with tea (Camellia sinensis) in Shizuoka, central Japan, Soil Biol
Biochem, 77, 276-291, 2014.

1225 **Tables and Figures**

1230

Sformatowano: Legenda

pathway	$\delta^{15}N^{SP}$	literature values $\varepsilon^{18}O$	$\varepsilon^{15}N$	reference	substrate isotope values $\delta^{18}O_{H2O}$	$\delta^{15}N_{field}$	$\delta^{15}N_{lab}$	**substrate corrected values** $\delta^{18}O$	$\delta^{15}N_{field}$	$\delta^{15}N_{lab}$
bD	**-1.9±4.6**	19.0±2.1	-45.8±4.7	(Barford et al., 1999; Lewicka-Szczebak et al., 2016; Lewicka-Szczebak et al., 2014; Rohe et al., 2017; Sutka et al., 2006; Toyoda et al., 2005)	-6.4	11.9	4.5	**12.6±2.1**	**-33.9±4.7**	**-41.3±4.7**
nD	**-5.9±6.5**	15.7±2.9	-56.9±3.8	(Frame and Casciotti, 2010; Sutka et al., 2006)	-6.4	41.4	79.3	**9.3±2.9**	**-15.5±3.8**	**22.4±3.8**
fD	**33.6±2.5**	46.9±3.8	-38.0±6.6	(Maeda et al., 2015; Rohe et al., 2014a; Rohe et al., 2017; Sutka et al., 2008)	-6.4	11.9	4.5	**40.5±3.8**	**-26.1±6.6**	**-33.5±6.6**
Ni	**35.0±2.9**	23.5±2.1	-57.0±7.3	(Frame and Casciotti, 2010; Mandernack et al., 2009; Sutka et al., 2006; Yoshida, 1988)		41.4	79.3		**-15.6±7.3**	**22.3±7.3**
reduction	**-6.0±1.4**	**-15.9±4.7**	**-7.0±2.1**	(Jinuntuya-Nortman et al., 2008; Lewicka-Szczebak et al., 2015; Lewicka-Szczebak et al., 2014; Menyailo and Hungate, 2006; Ostrom et al., 2007; Well and Flessa, 2009)						

38

Table ~~1~~ 2: Results summary

	treatment	F1	F2	F3	L1	L2
WFPS [%]		65.1±4.3	69.1±4.5	62.4±4.1	60→65	70→80
N_2O flux [gN-N_2O ha^{-1}d^{-1}]	NA	8.9±7.4	16.3±26.1	331.3±302.9	4.9±4.7	8.5±5.6
	^{15}N	5.9±5.5	4.3±3.3	330.9±323.7	1.4±1.0	54.6±50.2
N_2 flux[a] [gN-N_2 ha^{-1}d^{-1}]	^{15}N	bd (<11.3)	108.2±84.1[b]	576.4±285.4	2~~63.63~~±1~~89.12~~	4~~53.34~~±44.5
r_{N2O}[a]	^{15}N	nd (>0.75)	0.06±0.04[b]	0.33±0.15	0.12±0.10	0.49±0.31
NO_3 content [mg N kg^{-1} soil]	NA	13.6±3.1	8.0±2.4	13.6±3.2	21.2±1.5	21.0±1.7
	^{15}N	15.8±6.2	7.5±1.1	15.8±5.5	20.1±0.6	19.4±1.1
NH_4 content [mg N kg^{-1} soil]	NA	3.8±2.1	6.4±3.3	3.4±1.5	0.53±0.19	0.71±0.23
	^{15}N	2.0±2.6	5.4±3.1	3.7±1.9	0.58±0.2	0.72±0.15
$\delta^{15}N_{NO3}$ [‰]	NA	8.0±5.4	11.7±5.3	12.1±3.7	4.5±0.4	4.7±0.55
$\delta^{15}N_{NH4}$ [‰]	NA	31.0±8.7	40.5±6.8	42.2±9.1	90.0±7.9	70.4±17.9
$a^{15}N_{NO3}$ [atom %]	^{15}N	20.5±9.6	40.3±10.1	19.7±5.8	13.6±0.7	13.9±0.8
$a^{15}N_{NH4}$ [atom %]	^{15}N	0.7±0.6	0.9±0.4	0.5±0.2	0.5±0.03	0.5±0.01
$a^{15}N_{NO2}$ [atom %]	^{15}N	15.5±9.4	21.9±8.0	10.9±2.3	8.5±6.1	10.3±3.8
$\delta^{15}N_{N2O}$	NA	-33.4±9.5	-20.2±16.0	-14.0±14.8	-2.4±8.0	-17.7±11.9
$\delta^{18}O_{N2O}$	NA	22.7±4.3	33.2±5.6	33.4±6.1	40.8±5.5	36.8±5.2
$\delta^{15}N^{SP}_{N2O}$	NA	9.4±4.5	11.6±5.4	6.9±5.2	9.0±6.2	8.6±3.1
$a^{15}N_{N2O}$ [atom %]	^{15}N	7.5±2.7	11.7±7.3	16.2±10.6	11.8±0.72	13.7±0.67
f_{P_N2O}	^{15}N	0.28±0.12	0.23±0.13	0.59±0.19	0.69±0.06	0.96±0.09
a_{P_N2O}	^{15}N	0.28±0.07	0.47±0.09	0.26±0.11	0.17±0.02	0.15±0.01
a_{P_N2}	^{15}N	nd	0.23±0.11	0.33±0.11	0.21±0.07	0.18±0.06

[a] determined in ^{15}N treatments with gas-flux method

[b] half of data below detection limit
bd – below detection limit
nd – not determined – due to N_2 flux below detection limit

1240

40

Table 23: Comparison of N_2O residual fraction (r_{N2O}) determined with the N_2O isotopocule approaches (SP/O Map and 3DI model) and the reference method (^{15}N gas-flux). Minimal (min), maximal (max) and mean values were calculated with the each sampling mean values (of all replicates). The agreement with the reference method was assessed with the Nash–Sutcliffe efficiency (F, Eq. ~~17~~19) (Nash and Sutcliffe, 1970), which represent the R^2 of the fit to the 1:1 line (Fig. ~~7~~6).

|		N_2O isotopocule approaches				reference method
		SP/O Map		3DI model		^{15}N gas-flux
		Case1	Case2	Case1	Case2	
L1	min	0.15	0.14	0.41	0.16	0.03
	max	0.24	0.24	0.71	0.32	0.30
	mean	**0.19**	**0.18**	**0.49**	**0.21**	**0.12**
L2	min	0.16	0.15	0.40	0.17	0.12
	max	0.52	0.53	0.71	0.68	0.93
	mean	**0.27**	**0.27**	**0.49**	**0.36**	**0.50**
F1	min	0.68	0.70	0.89	0.87	0.75[a]
	max	1.00	1.00	0.93	0.93	1[a]
	mean	**0.86**	**0.86**	**0.91**	**0.89**	**nd[a]**
F2	min	0.30	0.36	0.46	0.22	0.02[b]
	max	0.43	0.49	0.72	0.61	0.11[b]
	mean	**0.38**	**0.42**	**0.58**	**0.39**	**0.06[b]**
F3	min	0.26	0.27	0.39	0.27	0.17
	max	0.47	0.47	0.82	0.42	0.59
	mean	**0.33**	**0.32**	**0.54**	**0.34**	**0.33**
agreement with reference method (F)		**0.59*** p=0.091	**0.61*** p=0.081	**-0.09**	**0.77**** p=0.015	

[a] all N_2 fluxes under detection limit, the range of values estimated based on detection limit – values not included in the statistics

[b] data not complete due to half of N_2 fluxes under detection limit – values not included in the statistics

Table ~~3~~ **4:** **Comparison of N$_2$O fraction originating from bD (f_{bD}) determined with the N$_2$O isotopocule approaches (SP/O Map and 3DI model) and the reference method (^{15}N gas-flux). Due to methodical assumptions for the particular approach either bD+nD fraction (for SP/O map and 3DI model) or bD+fD fraction (for 3DI model and reference method) can be compared (see Section 3.10).**

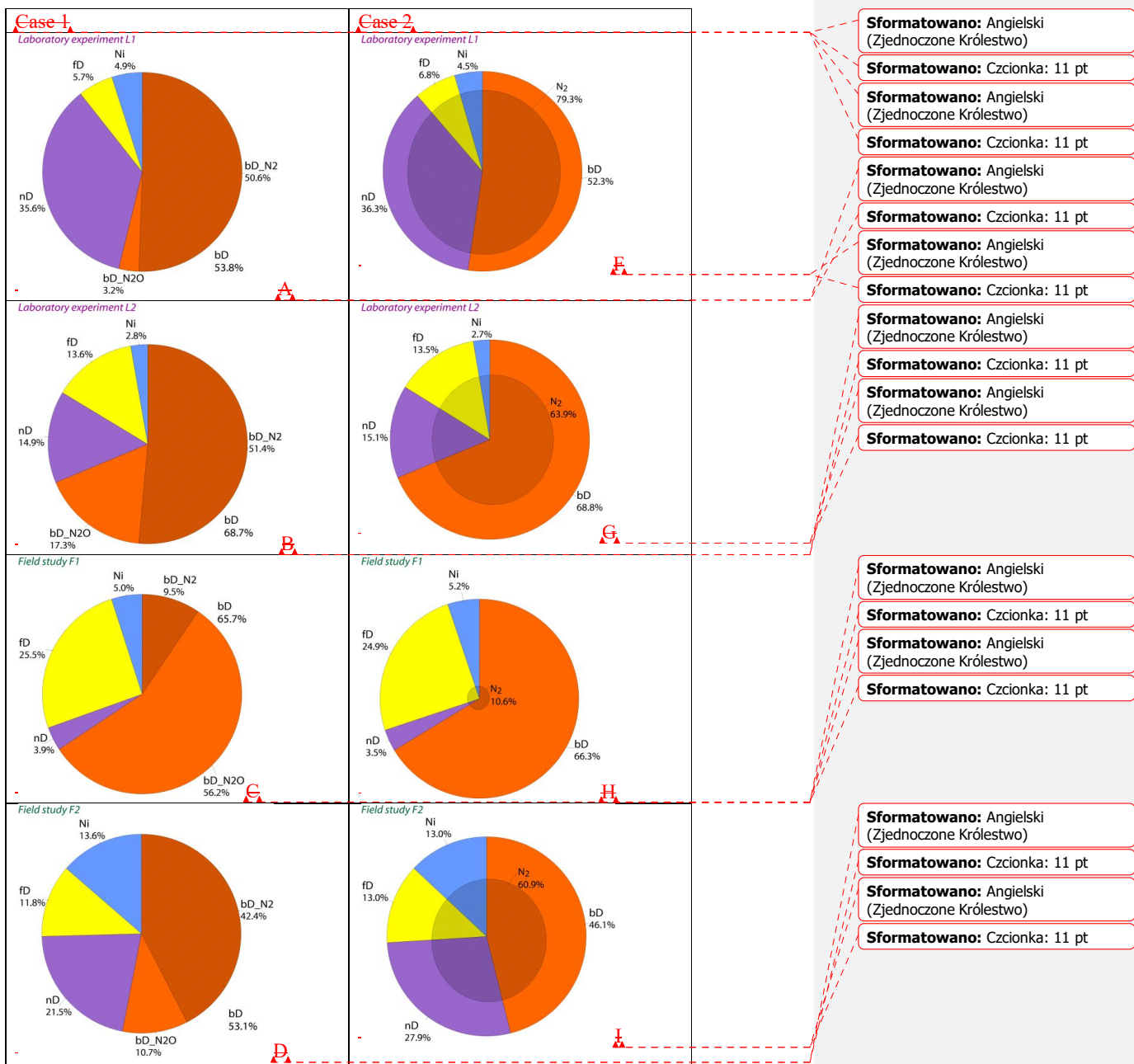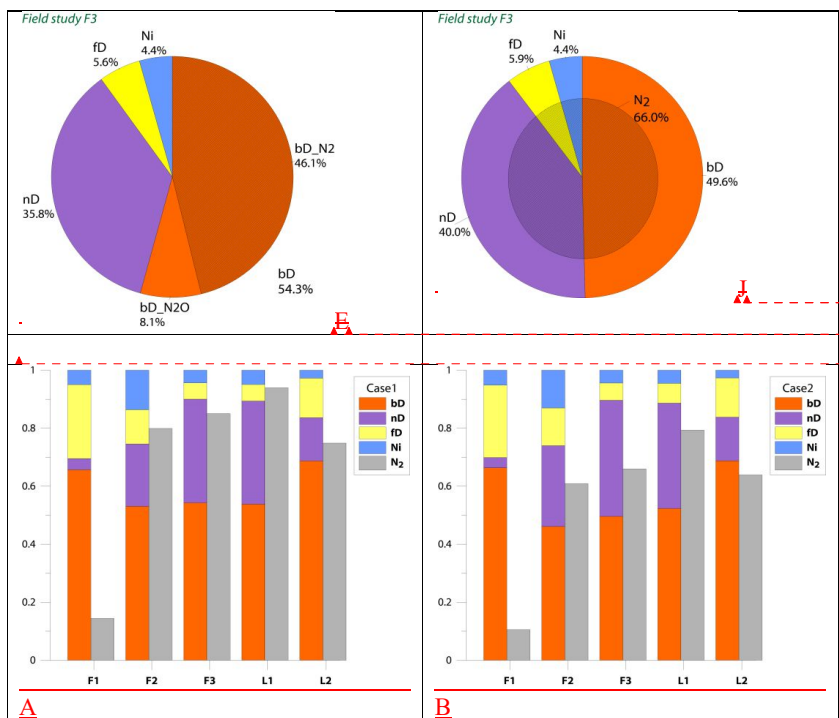|		N$_2$O	isotopocule					reference method
		approaches						
		SP/O Map (bD+nD)		3DI model (bD+nD)		3DI model (bD+fD)		^{15}N gas-flux (bD+fD)
		Case1	Case2	Case1	Case2	Case1	Case2	
L1	min	0.96	0.79	0.86	0.84	0.35	0.34	0.64
	max	1	1	0.94	0.94	0.71	0.71	0.75
	mean	**0.99**	**0.93**	**0.89**	**0.89**	**0.59**	**0.59**	**0.70**
L2	min	0.94	0.88	0.65	0.66	0.65	0.65	0.81
	max	1	1	0.95	0.95	0.97	0.97	1
	mean	**0.98**	**0.96**	**0.84**	**0.84**	**0.82**	**0.82**	**0.95**
F1	min	0.62	0.55	0.52	0.52	0.85	0.85	0.08
	max	0.84	0.83	0.82	0.82	0.97	0.97	0.42
	mean	**0.74**	**0.70**	**0.70**	**0.70**	**0.91**	**0.91**	**0.28**
F2	min	0.84	0.64	0.62	0.59	0.34	0.14	0.16
	max	0.95	0.89	0.83	0.83	0.94	0.95	0.31
	mean	**0.92**	**0.77**	**0.75**	**0.74**	**0.65**	**0.59**	**0.23**
F3	min	0.97	0.92	0.87	0.86	0.21	0.06	0.41
	max	1	1	0.93	0.93	0.92	0.92	0.83
	mean	**0.99**	**0.97**	**0.90**	**0.90**	**0.60**	**0.56**	**0.59**

1255
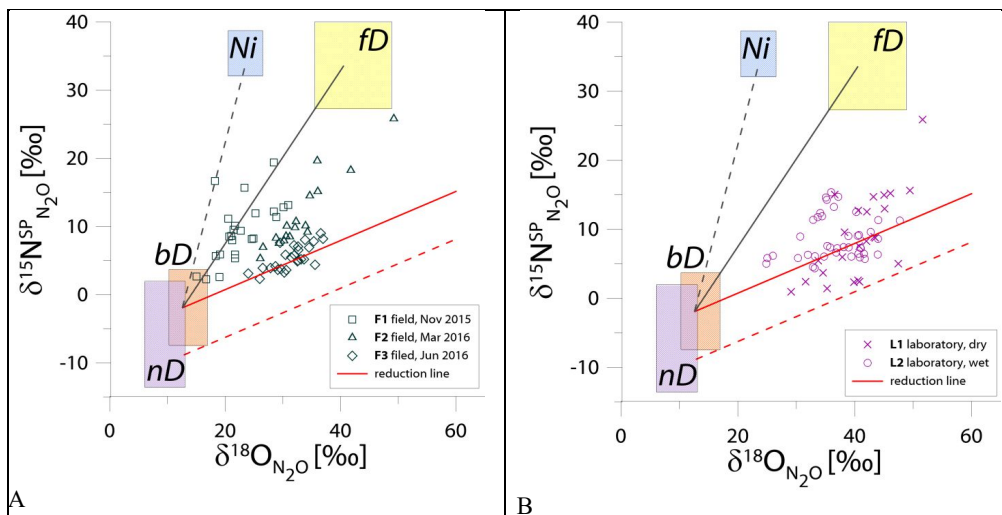
Fig.ure 1: N₂O isotope data of field (A, green points) and laboratory studies (B, purple points) in SP/O Map presented with literature endmember values and theoretical mixing (grey line) and reduction (red line) lines. The soild lines (bD-fD mixing and mean reduction line) are main assumptions used in the calculation procedures for SP/O Map. The grey dashed line shows the alternative bD-Ni mixing line (calculations with this alternative scenario are also presented in the supplement Table S1). The red dashed line shows the minimum reduction line – for the case of minimal delta values of the bD endmember. $\delta^{18}O$ values of mixing endmembers bD, nD and fD are presented in relation to the mean measured ambient water of -6.4‰ (hence present the expected $\delta^{18}O_{N_2O}$ originating from particular pathway in this study conditions).
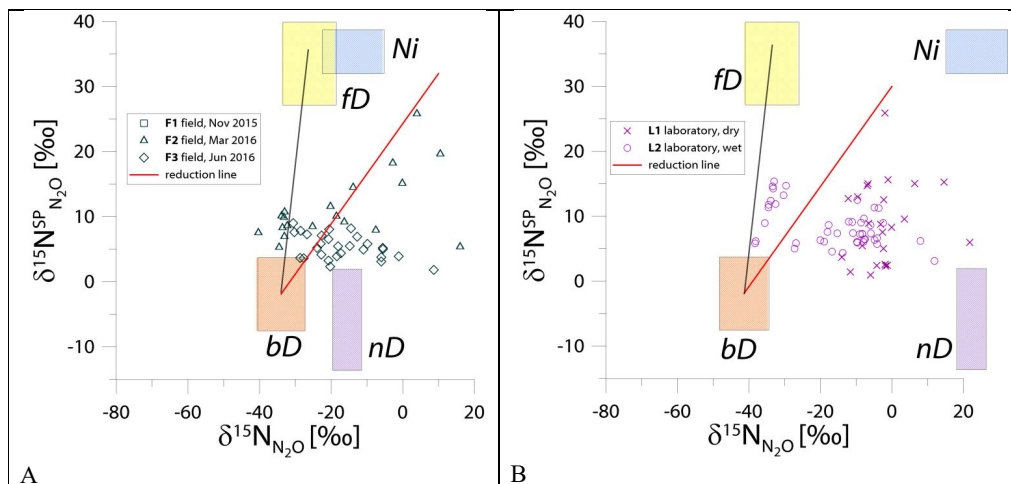
Figure 2: N₂O isotope data of field (green points) and laboratory (purple points) in SP/N Map presented with literature mixing endmember values and theoretical mixing (grey line) and reduction (red line) line. $\delta^{15}N$ values of mixing endmembers are presented in relation to the $\delta^{15}N$ of precursors: soil nitrate for bD and fD or ammonium for nD and Ni (hence present the expected $\delta^{15}N_{N2O}$ originating from particular pathway in this study conditions).
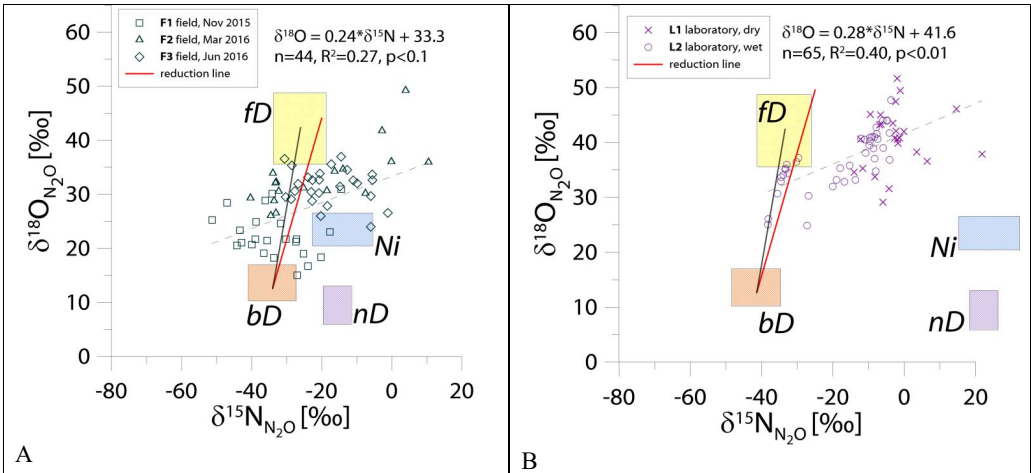
Figure 3: N₂O isotope data of field (A, green points) and laboratory (B, purple points) in O/N Map presented with literature mixing endmember values and theoretical mixing (grey line) and reduction (red line) lines. $\delta^{15}N$ values are presented in relation to the $\delta^{15}N$ of precursors: soil nitrate for bD and fD or ammonium for nD and Ni. $\delta^{18}O$ values of mixing endmembers bD, nD and fD are presented in relation to the mean measured ambient water of -6.4‰. Hence, the mixing endmember ranges present the expected $\delta^{15}N_{N2O}$ and $\delta^{18}O_{N2O}$ originating from particular pathway in this study conditions. The dashed line shows the linear fit for all the points with its equation and statistics above.

Case 1

Laboratory experiment L1

A

Laboratory experiment L2

B

Field study F1

C

Field study F2

D

Case 2

Laboratory experiment L1

E

Laboratory experiment L2

G

Field study F1

H

Field study F2

I

45

1280 **Fig~~ure:~~ 4: ~~Pie diagrams~~Bar plots showing ~~of~~ modeled ~~mixing ratios~~pathway fractions** (f_{bD}, f_{nD}, f_{fD}, f_{Ni}) **and N$_2$ flux contribution in the total (N$_2$+N$_2$O) flux (1-r_{N2O}). Results for both modeling cases: Case 1 (A~~-E~~) and Case 2 (~~BF-J~~) are shown. ~~Different graphical presentation of N$_2$ contribution reflects the different assumption for both cases: N$_2$ can be produced only from bD in Case 1, but N$_2$O from all pathways can be reduced to N$_2$ in Case 2. For both cases the percentage of N$_2$ is expressed in relation to the total (N$_2$+N$_2$O) flux.~~**
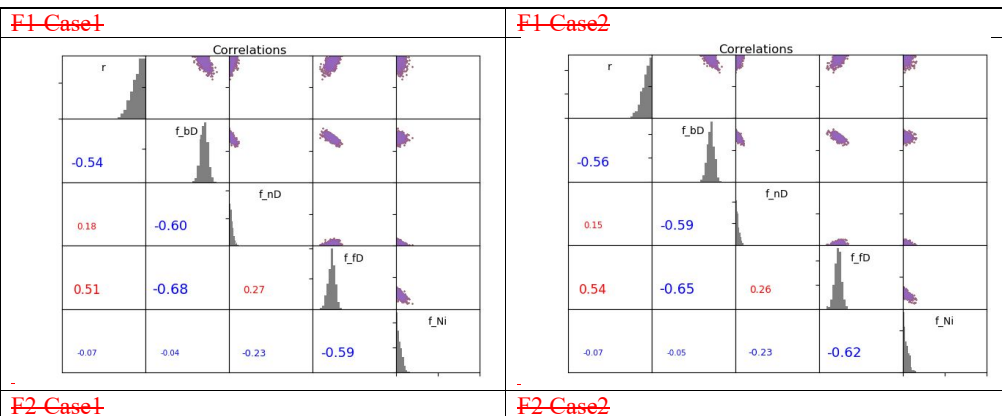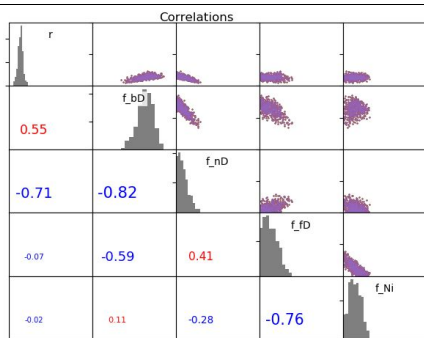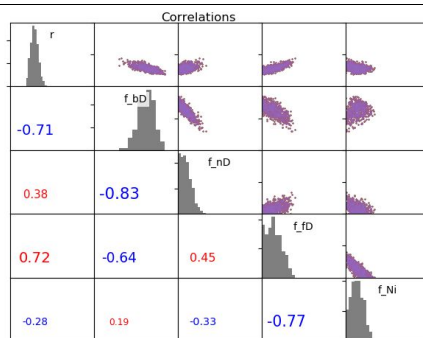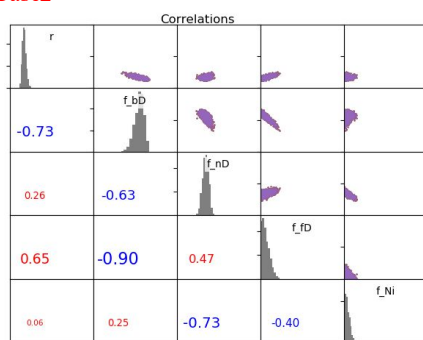
F3 Case1

F3 Case2
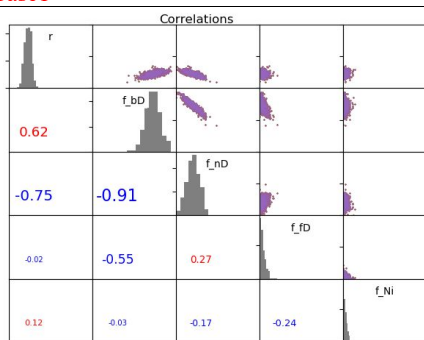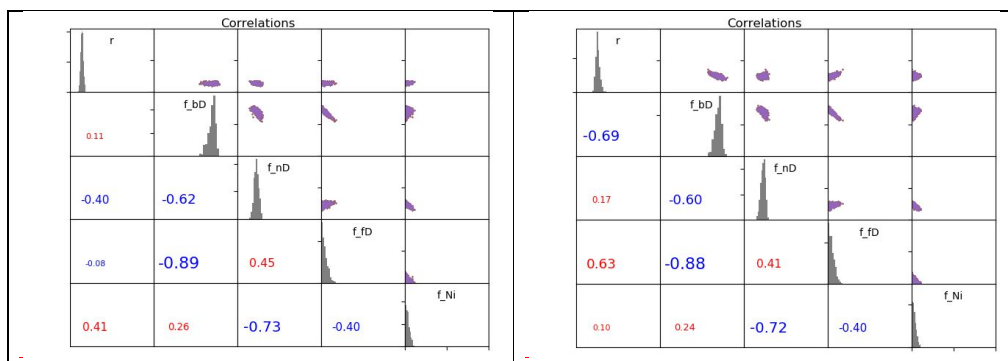

L1 Case1
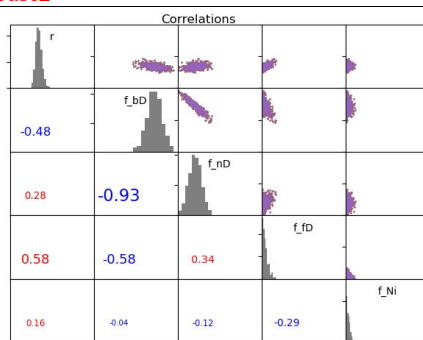

L1 Case2
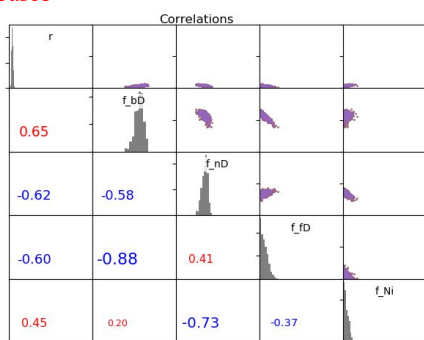
L2 Case1

L2 Case2

Fig. 5 Matrix plots presenting detailed 3DI model outputs for each sampling date – here representative examples for each sampling campaign are shown (in the supplement plots for all samples are shown. Fig. S4). The plots in the diagonal show histograms of posterior probability distribution of r_{N2O} and mixing ratios (scale from 0, left to 1, right), the plots above the diagonal show correlations between the modeled fractions (scale from 0, left to 1, right) and the values below the diagonal show R coefficient of these correlations: in blue for positive correlations and in red for negative correlations with the size proportional to the R value.

48
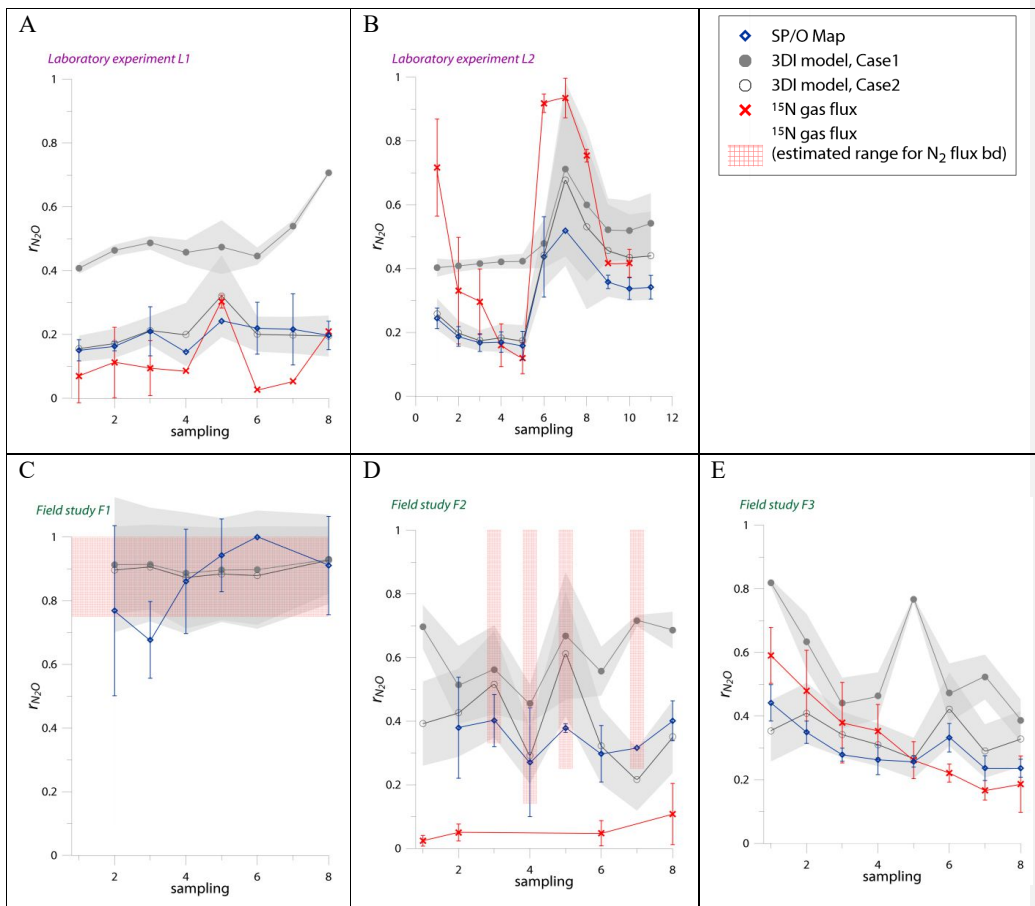
Figure.6 5: Comparison of time changes in residual N$_2$O fraction (r_{N_2O}) determined with O/SP Map Case 1 and 3DI model with the reference method (^{15}N gas-flux). For the 3DI model results the 95% confidence interval is shown with grey shaded areas. Error bars for O/SP Map and ^{15}N gas-flux data represent the standard deviation of replicate samples (n=4). For N$_2$ fluxes below the detection limit the estimated r_{N2O} values are shown (red areas), calculated with N$_2$ flux from 0 to 1 of the detection limit.

49
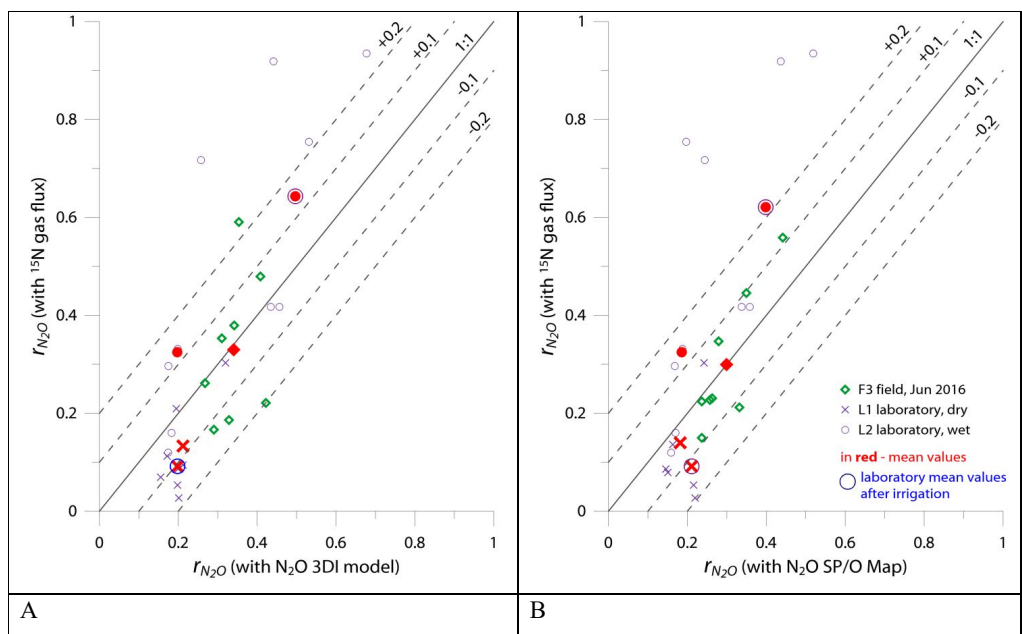
Fig~~ure.7~~ <ins>6:</ins> Comparison of 1:1 fit between r_{N2O} determined with the reference method (^{15}N gas-flux) and (A) 3DI model Case 2, (B) SP/O Map Case 1.
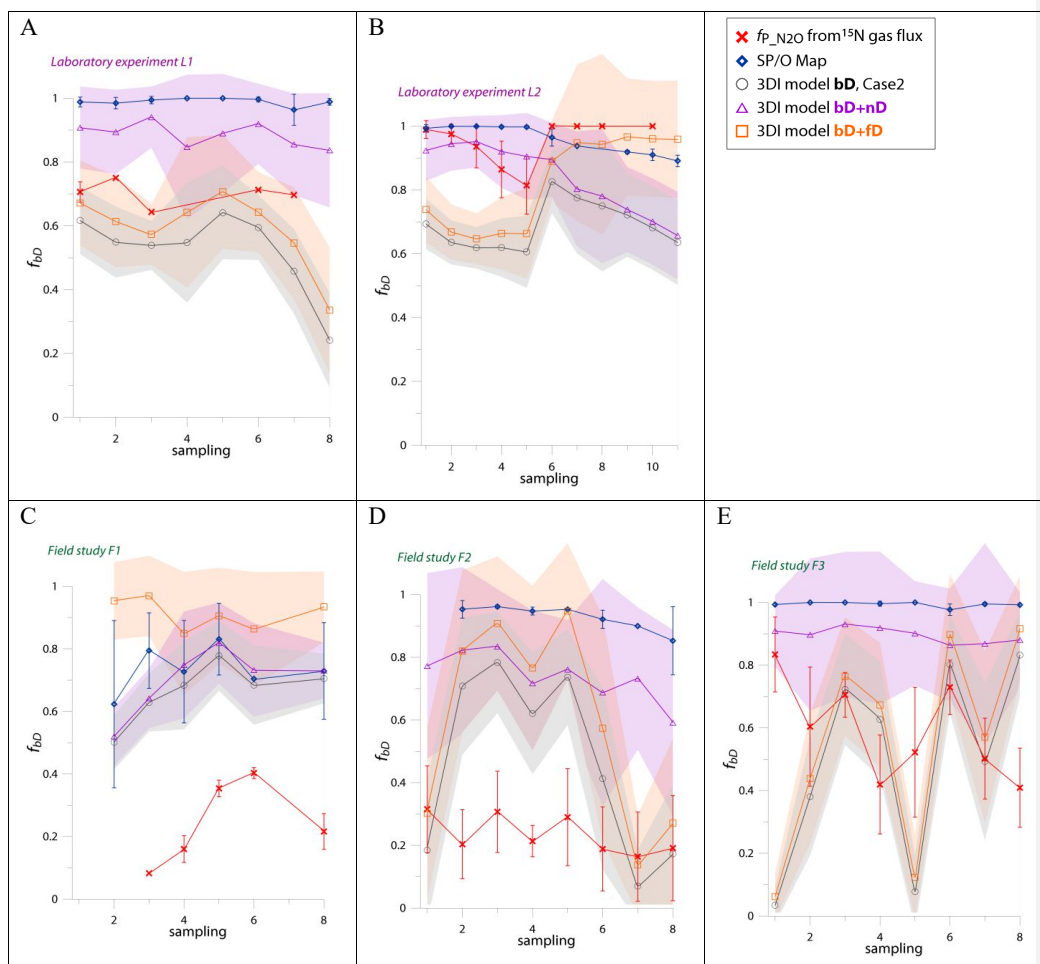
Figure.8 7: Comparison of N₂O fractions comprising bacterial denitrification (f_{bD}) determined with O/SP Map Case 1 (representing bD+nD) and 3DI model Case 2 (respective fractions determined: bD, bD+nD, bD+fD) with the reference method (^{15}N gas-flux). ^{15}N gas-flux method determines the f_{P_N2O} − ^{15}N-pool derived fraction − comprising all N₂O origins utilizing ^{15}N-labelled NO_3^- − theoretically mostly bD and fD. See Sections 4.2 and 4.3 for further discussion. For the 3DI model results the 95% confidence interval is shown with shaded areas. Error bars for O/SP Map and ^{15}N gas-flux data represent the standard deviation of replicate samples (n=4).

51